Studies on Chemical Structural Change of Pyrolyzing Coal and Real-time Analysis of Volatiles

張, 露

https://doi.org/10.15017/1866325

Studies on Chemical Structural Change of Pyrolyzing Coal and Real-time Analysis of Volatiles

by

Lu Zhang

Department of Applied Science for Electronics and Materials

Interdisciplinary Graduate School of Engineering Sciences

Kyushu University

2017

Contents

Chapter 1

General Introduction

1.1. Pyrolysis

Coal is the most abundant fossil fuel in the world [1]. Worldwide, coal continues to dominate the energy supply in future and play an increasing role particularly in developing countries. Pyrolysis is the initial step in most coal conversion processes, accounting for up to 70% of the weight loss suffered by the coal. It is also the process that is most dependent on the organic properties of the coal, and is important because of its influence on the subsequent conversion process. For example, the volatiles often control the ignition, the temperature and the stability of the flame. In addition, the pyrolysis process controls swelling, particle agglomeration, char reactivity, and char physical structure [2]. Soot formation is controlled by the tar produced in pyrolysis. In gasification, the product distributions are strongly influenced by pyrolysis. The pyrolysis process also controls the initial fragmentation of the macro-molecule in liquefaction. Accurate quantitative descriptions of coal pyrolysis in combustion are also important for the development of new pollution control strategies.

1.2. Technologies of coal conversion

Converting coal to a conventionally acceptable liquid or gaseous fuel can remedy its deficiencies compared with others fuel source such as oil and gas. The products of the conversion process can be comparable to oil and gas but not necessarily the same in all respects. That is, a particular conversion process can be chosen to improve a particular property of coal depending on its projected use.

1.2.1. Combustion

Throughout history, coal has been used to generate heat and to smelt metals. However, it was not until the 18th century that coal started to play an indispensable role in the economy. As an important fuel that propelled the industrial revolution [3,4], coal has been widely used since the 1700s to drive steam engines, in the operation of blast furnaces for metal production, in the production of cement, and in the generation of town gas for lighting and cooking. Since the late 19th century, coal has been used to power utility boilers for electricity generation [5]. Although its dominance as an energy source was replaced by crude oil in the 1950s, coal is still the single most important fuel for electricity generation today, accounting for 40% of the electricity generated worldwide [6]. The dominance of coal in electricity generation is expected to continue well into the 21st century.

Coal pyrolysis is important in combustion. Pyrolysis exerts its influence throughout the life of the solid particle from injection to burnout [7]. The processes of soften and swell of coal are mostly

determined by pyrolysis. Reactions such as bond breaking and cross-linking can be drastically influenced by chemical changes in the coal induced by weathering. The swelling of the coal particle is caused by expanding bubbles of gaseous volatiles produced by pyrolysis in the viscous liquid. Depending on the heating rate, temperature, and particle size, either a particle may swell or the bubbles may rupture. Coal softening affects the porosity and internal surface area of the resulting char. Softening, therefore, affects the ignition, particle trajectory in the furnace, reactivity, and eventual fragmentation. The ignition of the coal may be due to heterogeneous oxidation of the particle or to homogeneous combustion of the pyrolysis volatiles. The relative rates of solid oxidation and volatile evolution determine which type of ignition occurs first. So understanding of coal pyrolysis is essential in that of combustion.

1.2.2. Gasification

Coal gasification can convert coal to a variety of products—e.g. hydrogen, liquid fuels and chemicals—besides electricity. Further, gasification is a preferred scheme from a pollutant and carbon management viewpoint. Unlike traditional combustion processes which fully oxidize carbonaceous fuels to generate heat, modern coal gasifiers convert coal into syngas via partial oxidation reactions with oxygen or with steam and oxygen under elevated pressures [8]. In the coal gasification process, coal first reacts with oxygen (and steam) to produce raw syngas. The raw syngas, with pollutants such as particulates, H_2S, COS, HCl, ammonia, and mercury, is purified before it is sent to a gas turbine–steam turbine combined cycle system for electricity generation.

As the process develops, it continues to face a number of problems and therefore continues to evolve following incremental developments and improvements. A challenge in gasification research is that many of the assumptions in kinetic modeling have not been clearly presented, and the understanding of the implicit considerations of every single model is an onerous task [9].

1.2.3. Liquefaction

During the process of liquefaction, solid coal is converted to liquid fuels, such as gasoline, jet fuel, distillate fuel, or residual fuel [10,11]. There are two approaches to coal liquefaction: direct and indirect [12]. For direct liquefaction, crushed coal is slurried in a process-derived oil and reacted directly with hydrogen under high pressures and temperatures. Direct liquefaction has several processes and the end-products depend on the reactor conditions, the degree of hydrogenation-severity, and the nature of the process itself. Direct liquefaction can produce a range of products from gas to solid solvent-refined coal. This variation in conversion processes leads to confusion in evaluating and comparing the economics of the various processes. At high severities of

hydrogenation, the product can be so similar that it is almost indistinguishable from natural oil. In indirect liquefaction, coal is gasified to produce syngas, a mixture of hydrogen and carbon monoxide, and then combined in the presence of catalysts to form liquid compounds.

1.3. Analysis methods of gas products

To analyze the gas produced from coal pyrolysis, discrete samples of gas may be taken and then analyzed by a specialist laboratory. Such analysis can be done using gas chromatography (GC), or with an infrared (IR) system.

The main advantage of GC is that it can provide a quantitative data on the complicated gas, whereas its main drawback is the long measuring time. Therefore, it is not a suitable method for real-time analysis during transient operating conditions encountered in a gasification process. Also, even if a set of discrete samples were to be taken for subsequent analysis, then problems can often be encountered either, with possible leakage of species (e.g. hydrogen) from the sample container, or difficulties in the sampling process, both resulting in incorrect results.

Although IR spectroscopy could be used to perform measurements in real-time, its main disadvantage arises from the fact that, in general, it measures a single gas species, and hence information on the other key components in the gas mixture is missing. It is therefore not unusual to find in the literature that a combination of GC and IR techniques is used. For example, Craig [13] reports the use of both methods, using a non-dispersive infrared analyzer to monitor continuously levels of CO and CO_2. The concentrations of the other gases e.g. H_2, CH_4, NOx, O_2 were obtained from measurements on samples taken every 15 min, and the GC was one of the analytical instruments used. Other researchers [14] used the non-dispersive infrared analysis technique to measure the composition of the gas produced from an Imbert downdraft gasifier. However, only five gases were analyzed (CO, H_2, CO_2, CH_4, N_2), providing information on gas composition at 1 min intervals.

In the literature, there is evidence of an interest (and hence need) to perform in real-time analysis of the gas produced. In Karlegärd et al. [15], the use of quadrupole mass spectrometry (QMS) for real-time analysis of gas (from gasification process) was reported. Nevertheless, this method was limited due to its complexity, and it was only tested for a very narrow range of concentrations of species in the gas. Although QMS is already used in many industries, its use for the analysis of fuel gas streams is not so widespread [16]. In addition, despite being a well-established technique, there are still some technical difficulties in using it for the real-time analysis of multicomponent gas mixtures.

1.4. Analysis methods of tar

There are a few methods sampling and measuring the tar formation, such as solid phase adsorption and cold trapping, GC, liquid Chromatography (LC), GC/MS and FT-IR. Fujioka adopted GC/MS to analyze the main ingredients in tar, and used the methods of electron impact (EI), chemical ionization (CI) and nitrogen chemical ionization (N-CI) to measure the samples of aromatics, respectively; indicating that the sensitivities of polyaromatics are not apparent different and the sensitivities of alkylaromatics are low. FT-IR was also used to measure the coal tar, indicating there were more than 30 compounds of which weight percent was higher than 1% and most of them were aromatics. Many compounds can be detected accurately; however, some species were difficult to be detected due to the low sensitivity of FT-IR. Compared with other measurement methods, mass spectrum is still the best methods monitoring of the product gas in the gasifiers accurately [17-19]. There are several traditional patterns of ionization, such as EI and CI, but such ion sources would create fragment ions. In multi-component system, such as coal/biomass gasification, these ionization methods are not suitable [20]. Moreover, it is impossible for EI and CI to real-time monitor without pretreatment of the samples. To overcome above shortages, some soft ionization methods were created, such as electrospray ionization [21-24] and matrix-assisted laser desorption ionization [25-28], which makes it possible to real-time monitor without pretreatment of the samples.

Ion attachment mass spectrum (IAMS) can be looked on as one of ESIs and the sample ion is, therefore, less likely to fragment and more information about the intact sample molecule may be obtained. An added advantage of this technique is that direct determination of unstable, intermediary, and reactive species is possible. Sensitivity is high because of the ion-molecule reactions. Studies on the ion chemistry of various metal ions with various classes of molecules have been done. Fujii et al. [29] investigated the application of In^+ ions in IAMS. However, alkali ions, especially Li^+ ions, have still been mainly utilized as primary ions since they can be readily generated by thermionic emission. Juhász et al. [30] used IAMS to study the thermal degradation of solid vitamin C, indicating that the occurrence of secondary reactions of the primary pyrolysis products was greatly reduced and some decomposition products were detected by IAMS for the first time. Fujii et al. [31] used Li^+ IAMS to detect copper organic complex, a thermally labile precursor used for Cu-CVD. IAMS was promising for real-time monitoring of by-products in the Cu-CVD process. In addition to the detection of molecules, IAMS was even used to study free radicals. Kitahara et al. [32] used Li^+ IAMS to study the gas-phase hydrocarbon free radical species produced during thermal irradiation of polyethylene polymers, confirming the formation of various kinds of HC radicals up to C_{12}. Using direct probe-Li^+ IAMS to study Japanese lacquers, Tsukagoshi et al. [33] put forward a question whether it is valid to

assign peaks as aromatics, aliphatics, acids and phenolics or not. Indeed, this is a big limitation for the current quadrupole system used in analyzer [34].

1.5. Objective and outline of this study

Pyrolysis is a most generally used technology for down-stream processing and clean utilizations of coal. Pyrolysis of coal produces three main products, i.e., light gases, tar, and char. Deep insight into the reaction processes during the coal pyrolysis is critical to develop this technology. Real-time analysis is a most effective approach to explore the mechanisms of the pyrolysis accurately, however, has not been sufficiently developed. In addition, the study on the detailed processes of coke formation during the coal pyrolysis is an attractive subject to coke industry, and also an important topic to the community of the low rank coal utilization. In this thesis, the author applies a series of off-line characterizations to coal-to-coke, in order to explore the chemical structural change of coal during the pyrolysis, and carries out the real-time quantitative analysis to volatiles from the pyrolysis.

Chapter 1 reviews existing technologies for the coal pyrolysis, real-time analysis, and also so for proposed models of chemical structure of coal and its pyrolysis mechanism.

In order to study the chemical structural change of coal during the pyrolysis, in Chapter 2, the samples of caking coal (CC), non-caking coal (NCC) and their cokes which were gotten from pyrolyzing coal at the temperature range from 400 to 900 ℃ were evaluated by solid state ^{13}C-NMR, FT-IR, XPS and Raman, respectively. Sizes of aromatic clusters with pyrolyzing coal were estimated via ^{13}C-NMR. It was found that CC has less substituents, but higher aromaticity and condensation degree than those of NCC. During the pyrolysis, NCC would be deprived more substituents and then produced more gases than CC to evolve an aromatic structure similar to CC. Eventually, it was impossible to distinguish the coking products of NCC and CC in terms of both aromaticity and condensation degree. Other three characterizations indicated that, compared with CC, NCC contained more O-containing functional groups, in particular hydroxyl and ester groups, which were related to the cross-linking reactions during the pyrolysis. It was also found that those reactions related to O-containing groups mainly occur before 500 ℃.

In Chapter 3, to investigate the strict relationship between the substituents or functional groups attached to the coal macromolecules and the generation of the volatile products, e.g., CH_4, H_2O, CO, CO_2, etc., during the coal pyrolysis, quadrupole mass spectrometry, gas chromatography, and ^{13}C nuclear magnetic resonance were applied to real-time monitoring the formations of volatile products, off-line quantitative determination of the total products from the pyrolysis of NCC, and the changes of diverse substituents in the NCC along with coke formation, respectively. These measurements were also performed for the pyrolysis of CC to contrast NCC. Qualitative formation rates as a

function of temperature of gas products were achieved, and then were deconvoluted and assigned to several peaks based on the possible reactions occurred during the pyrolysis. These data revealed that, during the pyrolysis, the functional groups related to the formation of CO, i.e., ether, carbonyl, and anhydride, can directly generate CO via bond breaking, or take a detour of the formation of other intermediates via condensation and recombination firstly. Moreover, the formations of CO_2 and CH_4 were related to the direct removal of -COO- and -CH_3, respectively.

In order to real-time analyze the formation of tar during the coal pyrolysis, Chapter 4 describes a prototype device for Li^+ ion-attachment mass spectrometry (IAMS) was developed for real-time quantitative monitoring of the vapor produced from thermochemical conversion of coal. Simulated tar vapor containing a suite of aromatics and the real vapor produced from the pyrolysis of coal were monitored by IAMS with a Li^+ source. It was confirmed that both the simulated and real vapors are ionized without undergoing fragmentation and the sensitivities of these detected aromatic molecules are similar to one another. In addition, when the feeding rate of the coal sample was changed from 0.5 to 1.0 g/min, the peak intensities increased nearly twice as much. These results showed the possibility of applying IAMS to the quantitatively monitoring of coal-derived volatiles.

The general conclusions of this thesis are proposed in Chapter 5. First, during the pyrolysis, NCC was removed more substituents and then produced more gases than CC to evolve a coke structure. Second, during the coal pyrolysis, the CO formation can be mainly attributed to the cleavage of ether group, the removal of anhydrides, oxygen free radicals reaction, and cleavage of carbonyl groups. The removals of carboxyl, ester, and anhydride groups were the main reasons for the CO_2 formation. The quantity of aromatic oxygen during the pyrolysis would temporarily increase due to some secondary reactions, as well as the quantity of aliphatic oxygen. Third, the advantages (no occurrence of fragmentary ions) of Li^+−IAMS enabled real-time qualitative analysis of the simulated tar vapor. Li^+−IAMS performed well to the quantitative analysis of the simulated tar vapor because of its equivalent sensitivities of the aromatics with Li^+ affinities above 1 eV. Moreover, the results of real vapor from the coal pyrolysis monitored by Li^+−IAMS coincided very well with those of the simulated tar vapor.

1.6. References

1. M. A. Elliott, G. R, Yohe. *Chemistry of coal utilization.* New York: Wiley-Interscience, 1981, 1–52.
2. P. R. Solomon, T. H. Fletcher, R. J. Pugmire, *fuel*, 1993, **72**(5), 587-597.
3. T. S. Ashton, Oxford University Press, New York, 1997, 1760-1830.
4. R. Chruch, Clarendon Press, Oxford, 1986, **3**, 1830-1913.

5. S. C. Stultz, J. B. Kitto, The Babcock and Wilcox Company, Barberton, Ohio, 40th edn, 1992.
6. International Energy Outlook 2007. EIA, U.S. Department of Energy, Washington DC, 2007.
7. P. R. Solomon, T. H. Fletcher, *Twenty-Fifth Symposium (International) on Combustion/The Combustion Institute*, 1994, 463-474.
8. C. Higman, Gasification, Gulf Professional, Boston, Massachusetts, 2nd edn, 2008.
9. N. Mahinpey, A. Gomez, *Chem. Eng. Sci.*, 2016, **148**, 14-31.
10. H. F. Shui, Z. Y. Cai, C. B. Xu, *Energies*, 2010, **3**(2), 155-170.
11. S. Vasireddy, B. Morreale, A. Cugini, C. H. Song, J. Spivey, *Energy Environ. Sci.*, 2011, **4**, 311-345.
12. T. Y. Yan, *Energy*, 1986, **11**, 1239-1247.
13. J. D. Craig, Contract 55018a, of the western regional biomass energy program, Texas; December 31, 2001.
14. N. S. Mamphweli, E. L. Meyer, *Int. J. Energy Environ.*, 2010, **1**(1), 113-120.
15. A. Karlegärd, A. Götz, I. Bjerle, *Chem. Eng. Technol.*, 1995, **18**(3), 183–192.
16. K. D. Cook, K. H. Bennett, M. L. Haddix, *Ind. Eng. Chem. Res.*, 1999, **38**, 1192–1204.
17. R. J. Evans, T. A. Milne, *Energy Fuel*, 1987, **1**, 123-137.
18. R. J. Evans, T. A. Milne, *Energy Fuel*, 1987, **1**, 311-319.
19. P. Hasler, T. Nussbaumer, *Berne: Swiss Federal Office of Energy*, 1997.
20. M. Y. Dong, Y. H. He, Z. B. Zhu, *J. ECUST.*, 2000, **26**, 309-314.
21. I. Moraleja, E. Moreno-Gordaliza, M. L. Mena, *Talanta*, 2014, **120**, 433-442.
22. S. Devari, S. Jaglan, M. Kumar, *Phytochem.*, 2014, **98**, 183-189.
23. X. Wang, Y. Z. Liu, H. D. Wang, *Talanta*, 2013, **116**, 368-375.
24. M. L. Mena, E. Moreno-Gordaliza, M. M. Gómez-Gómez, *Talanta*, 2013, **116**, 581-592.
25. X. H. Yang, T. Wu, B. X. Liu, *Int. J. Mass Spectrom.*, 2013, **356**, 1-6.
26. G. B. Deacon, L. D. Field, K. Fisher, *J. Organomet. Chem.*, 2014, **751**, 482-492.
27. S. B. Jayasinghe, J. A. Caruso, *Int. J. Mass Spectrom.*, 2013, **356**, 33-36.
28. B. Fuchs, K. Bresler, J. Schiller, *Chem. Phys. Lipids*, 2011, **164**, 782-795.
29. T. Fujii, S, *Int. J. Mass Spectrom.*, 2000, **198**, 15-21.
30. M. Juhász, Y. Kitahara, T. Fujii, *Food Chem.*, 2011, **129**, 546-550.
31. T. Fujii, S. Arulmozhiraja, M. Nakamura, *Chem. Phys. Lett.*, 2006, **425**, 134-137.
32. Y. Kitahara, M. Tsukagoshi, S. Takahashi, *Chem. Phys. Lett.*, 2011, **507**, 226-228.
33. M. Tsukagoshi, Y. Kitahara, S. Takahashi, *J. Anal. Appl. Pyrol.*, 2012, **95**, 156-163.
34. B. Saini, G. Bansal, *J. Pharmaceut. Biomed.*, 2013, **84**, 224-231.

Chapter 2

Analysis of chemical structure of pyrolyzing coals using high resolution solid state ^{13}C-NMR, FT-IR, XPS and Raman

2.1. Introduction

Coal is a highly complex and heterogeneous material whose physical and chemical properties are different to be determined. Chemical structures of the organic molecule in coal vary greatly, particularly with its rank, to the extent that coals even from the same region might show more differences than similarities. Physical properties of coal generally vary so systematically with coal rank that it might be possible to reasonably predict the carbon content of the volatile matter of the coal. Understanding of chemical structures coal can be achieved by the understanding of the products during coal devolatilization. The physical structure of the main product–char changes significantly while volatile matter is generated during the devolatilization [1]. To investigate the coal-to-char evolution, a series of advanced technologies for coal utilization are carried out in this study.

Solid-state ^{13}C nuclear magnetic resonance (NMR) spectroscopy is a convenient, nondestructive tool for the analysis of chemical structure of solid fossil fuels [2]. By the use of cross-polarization [3], magic-angle-spinning, and dipolar-decoupling techniques [4], a direct measurement of the relative number of aromatic and nonaromatic carbons is possible [5]. Since Bartuska first reported high-resolution solid-state ^{13}C NMR spectra of coals [6], it was then applied to characterize the organic matter in oil shales, humic substances, kerogens, and their precursor biopolymers for several decades. Recently, great achievements have been made in the investigation of hydrocarbon-generating potential, structural evolution, organic carbon composition, and oil- and gas-generating mechanisms of coals, oil shales, and kerogens [7-10]. It has become one of the most powerful research tools to elucidate the chemical structures of complex macromolecules such as coal and char.

The ability to differentiate the kinds of organic oxygen is important for understanding both the utilization processes of coal and the formation of oxygen-containing products of coal pyrolysis. Fourier Transform Infrared (FT-IR) spectroscopy has been used for many years to get qualitative information of organic oxygen species [11,12]. X-ray photoelectron spectroscopy (XPS) is quantitative in nature, however the core level spectra of carbon tends to become heavily convoluted by multiple oxidation states. Many researchers dedicated to solve these difficulties for decades to analyze binding energy shifts associated with various heteroatoms including oxygen, nitrogen and fluorine are used to determine the elemental composition of the materials. There are also a number of publications [13-15] on the use of XPS for the study of chars. Kelemen [16] reports a method for

determining the level of aromatic carbon in which a mixed 70% Gaussian - 30% Lorntzin line shape and a peak width at half-maximum of 1.80 eV for each peak is used to curve resolve the carbon (1s) spectrum. Five peaks are resulting used in curve resolution that occur at 284.8, 285.3, 286.3, 287.5 and 289.0 (±0.1) eV. Raman spectroscopy is the most powerful technique to evaluate the structural features of carbonaceous materials, because it is sensitive to both the crystalline and amorphous structures [17]. It was widely used to explore the structural features of almost all carbonaceous materials [18]. In these studies, the Raman spectral characteristics, mainly those of the G (graphite) and D (defect) bands, were used to investigate the coal/char structure and its correlation to other characteristics.

In this study, in order to study the chemical structural change of coal during the pyrolysis, the samples of caking coal, non-caking coal and their cokes which are gotten from pyrolyzing coal at the temperature range from 400 to 900 ℃ are evaluated by solid state ^{13}C-NMR, FT-IR, XPS and Raman, respectively.

2.2. Experimental section

2.2.1. Samples

Caking coal (CC) and non-caking coal (NCC) are used in this study. The proximate analysis of these two kinds of coal are as follows: NCC, moisture 4.9 wt.%, ash 1.2 d-wt.%, volatile 48.6 d-wt.%; CC, moisture 2.2 wt.%, ash 9.1 d-wt.%, volatile 23.1 d-wt.%. The coal samples are pulverized to less than 75 μm and dried under vacuum at 40 ℃ for 24 h.

2.2.2. Heat treated coals

Coal powders are briquetted at ambient temperature and with mechanical pressure of 128 MPa for 8 min. Each briquette (1.0 g, 14 mm of diameter) is heated up to different target temperatures ranging from 400 to 900 ℃ at heating rate of 5 ℃/min with a N_2 flowrate of 200 ml/min (STP) in a vertical quartz tube reactor for heat treatment coals, as shown in **Fig. 2.1**. Once reaching the target temperatures, the char briquettes are instantaneously cooled down by falling into the bottom of the reactor immersed in liquid N_2. Yields and elementary analyses of raw coals and their cokes at different heat treated temperatures are shown in **Fig. 2.2** and **Table 2.**1 Residual heat treated coals are then pulverized to powders for the characterizations by solid-state ^{13}C NMR spectroscopy, FT-IR, XPS, and Raman.

2.2.3. Analysis of coal samples and cokes

The NMR spectra are recorded with the DEPTH2 technique at 100.53 MHz in a JEOL ECA 400 spectrometer. The repetition time was 20 s. Magic angle spinning was performed at 15 kHz in the

commercial probe (JEOL 4 mm CPMAS). The ^{13}C NMR data were then analyzed by a variation of the method described by Solum [19].

XPS analysis was carried out using an AXIS-165 spectrometer from Shimadzu/Kratos Co., Japan. The high-resolution XPS spectra of the sheet surfaces were obtained using a monochromatic AlKα X-ray source under the X-ray generation conditions at a voltage of 12 kV and a current of 5 mA. Energy corrections were made to account for samples charging based on the carbon (1s) peak at 284.8 eV [16]. Five peaks were used in curve fitting that occur at 284.4, 285.3, 286.3, 287.5 and 289 (±0.1) eV. The 284.8 eV peak represents contributions from both aromatic and aliphatic carbon. The 286.3 eV peak represents carbon bound to oxygen by a single bond (e.g., ethers, hydroxyls, etc.), the 287.5 eV peak corresponds to carbon bound to oxygen by two oxygen bonds (carbonyl), and the 290.0 eV peak corresponds to carbon bound to oxygen by three bonds (carboxyl) [16,20].

The FT-IR spectra of the coal samples and cokes were recorded on a FT-IR spectrometer (PerkinElmer Spectrum Two) with universal attenuated total reflectance (UATR) accessories. The UATR employs a DiCompTM crystal, which is composed of a diamond ATR with a ZnCe focusing element. The scan was conducted in the range from 4000 to 450 cm^{-1} at a resolution of 1 cm^{-1}.

Raman spectrum were obtained with a JASCO NRS-3000 Raman spectrometer (JASCO Corporation, Tokyo, Japan) and were then curve-fitted into 8 peaks based on the previous reports [21,22]. The assignments of these 8 bands located at the region of 1000-1800 cm^{-1} were briefly summarized in **Table 2.3**. In Raman spectra, the G band at 1598 cm^{-1} and the D band 1382 cm^{-1} are usually referred to as the Graphite and Defect bands respectively. In this study, in addition to these two bands, 6 other bands were employed to curve-fitting, including G_R (standing for G right), G_L (standing for G left), V_R (standing for valley right), V_L (standing for valley left), S (standing for on the side of the D band), S_R (standing for S right). All the samples investigated in this study were obtained by the optimum fitting results.

2.3. Results and discussion

2.3.1. NMR analysis

The spectra of ^{13}C-NMR are shown in **Fig. 2.3**. The peaks of vibrational aliphatic carbons are located within 0-60 ppm, and those within 100-170 ppm are ascribed to the vibrational aromatic carbons. With increasing the temperature of pyrolysis, the peaks indicating the presence of aliphatic carbons decrease gradually, while those of aromatic carbons increase correspondingly. This means that the aliphatic carbons are dissociated to be molecular fragments or transformed to aromatic carbons during the pyrolysis. Compared with NCC, there are less aliphatic carbons and O-containing

substituents in CC. Both CC and NCC will gradually lose their aliphatic carbons and the substituents during pyrolysis. In order to analyze the organic carbon varieties in the molecules of coal samples and cokes, ^{13}C NMR spectra are deconvoluted based on the chemical shifts shown in **Table 2.2** [19,23]. With the help of elemental analysis of coal samples (**Table 2.1**), the organic carbons can be classified quantitatively into 8 varieties, i.e., methyl ($-CH_3$), methylene ($-CH_2$), aliphatic carbon with oxygen substituents (Al-O), protonated aromatic carbon (Ar-H), aromatic carbon with alkyl groups (Ar-C), bridgehead carbon, aromatic carbon with oxygen substituents (Ar-O), and carbonyl carbon (O=C-O, C=O). The distribution of the organic carbons of the raw coal and cokes heat treated in elevated temperature are given in **Fig. 2.4** to **2.9**. **Fig. 2.4** and **2.5** show the total amount of carbons and aliphatic carbon structural distribution. CC as the higher rank than NCC has more total carbons and less alkane substituents in raw coal. During the decomposition, carbon number of CC decreases by less than 18%, while NCC decreases by around 31%.

Fig. 2.6 and **2.7** indicate the distribution of aromatic carbons in NCC and CC. Condensation among aromatic rings occurred with the pyrolysis of coal, which will increase the quantity of bridgehead carbon and simultaneously reduce that of protonated aromatic carbon [19]. It is obvious that the quantity of bridgehead carbon of both NCC and CC are largely increased since 450 ℃, and condensation of CC occurred sharply since 450 ℃ as well. The distribution of carbons bonding with O of NCC and CC is shown in **Fig. 2.8** and **2.9**. The O-containing substituents in coal include ether, hydroxyl, carbonyl, ester, and carboxyl groups. Compared with CC, NCC contains more ether and hydroxyl groups bonding with aromatic rings, and more carbonyl, ester, and carboxyl groups. These O-containing groups are closely related to the cross-linking reactions during the pyrolysis of coal. Therefore, NCC will produce more small molecules containing O such as H_2O, CO, and CO_2 during pyrolysis. Such O-containing groups have not largely decreased until 700 ℃. This means cross-linking reactions should occur within the temperature range from 400 to 700 ℃.

Two parameters are derived from the distribution of organic carbons to characterize the coking, i.e., carbon aromaticity (f_a) and aromatic condensation degree (X_b) [23-26], where f_a is the percentage of carbon in aromatic groups, and X_b is the fraction of aromatic bridgehead carbons. As shown in **Fig. 2.10** and **2.11**, as for raw coal, the aromaticity is increased with the coal ranks [19]. The aromaticity of CC is higher than that of NCC, while pyrolysis plays a crucial role for increasing the aromaticity of coal. It is interesting that the elevated temperature influences the aromaticity of NCC markedly, while the aromaticity of CC at 400 ℃ is similar with that of the raw coal. The aromaticity of NCC increases so rapidly at the temperature range from 450 to 500 ℃ that even exceeds that of CC. Finally, the aromaticities of NCC and CC turn to be same with each other at the temperature above 600 ℃. **Fig. 2.11** displays the aromatic condensation degrees of the pyrolysis of NCC and CC. The

condensation degrees of both NCC and CC increase at the temperature range from 450 to 500 ℃, while that of CC increases much rapider than that of NCC. On the basis of the above-mentioned discussions, cross-linking reactions of NCC at relative low temperature will remove the functional groups to form new substituents such as ether and ester groups, but the size of the aromatic layer will thus not be increased. However, the cross-linking reactions of CC seldom occur, and the condensation among aromatic rings are favored, the size of aromatic layer is thus increased largely. The increased condensation degree of CC in this stage, therefore, must be higher than that of NCC. Note that both the aromaticity and condensation of coal are increased with the temperature range; however, there is no necessary relationship between them.

During pyrolysis, NCC has to be deprived more substituents and produces more gases than CC to evolve an aromatic structures similar to CC. Eventually, it has been impossible to distinguish the coking products of NCC and CC in terms of both aromaticity and condensation degree.

2.3.2. FT-IR analysis

The FT-IR spectra of NCC and CC and their derivative cokes are shown in **Fig. 2.12** and **2.13**. Three bands indicating the presence of O-containing groups are shown in the figures. The signals of O-H stretching (3300 cm^{-1}) and aliphatic C-O stretching (1200 cm^{-1}) of NCC are more intensity than those of CC. As for NCC, the signal of O-H stretching is sharply reduced before 500 ℃. The signal of aliphatic C-O stretching was gradually reduced before 700 ℃, and disappeared completely after 700 ℃. The strong signals of C=O stretching (1600 cm^{-1}) of both NCC and CC decrease before 700 ℃, and vanish after 700 ℃. The O-H stretching signal located at 3300 cm^{-1} combined with the presence of C=O, the presence of –COOH can thus be verified in NCC. In CC, the C=O mainly exists as ester and carbonyl groups. Compared with CC, there are significant amount of –OH and –COOH groups in NCC. These functional groups will cause cross-linking reactions at high temperatures. The aliphatic C-O stretching signal located at 1200 cm^{-1} shows that NCC containing of more ether groups than CC. Besides, there is a strong peak at around 1000 cm^{-1} of CC which shows big difference from NCC. This peak can be attributed to Si-O stretching along with another sharp peak at about 470 cm^{-1} [27]. Overall, the results of FT-IR indicate again that NCC has much more oxygen-containing groups which including both C to O with a single band and C to O with a double band in raw coal than CC.

2.3.3. XPS analysis

As shown in **Fig. 2.14**, both the XPS spectra of NCC and those of CC can be mainly deconvoluted to five peaks, indicating the presence of chemical bonds of aromatic carbon, C-N, C-O, C=O, and

O=C-O, respectively. With elevated the temperature, the peaks of C-O and C=O of both NCC and CC decrease. This means the O-containing functional groups were continuously removed during pyrolysis, and some small molecules containing O are thus formed, such as H_2O, CO_2, and CO. When the temperature is elevated above 600 ℃, the peaks indicating the presence of C-O or C=O almost vanish, and only chemical bonds of aromatic carbons are remained. This means majority of the O-containing substituents have been removed at the temperature above 600 ℃, and the embryonic structure of coke are simultaneously formed. In other word, the carbon skeleton or aromatic nucleus of both NCC and CC are condensed in large scale. Compared with the XPS spectra of NCC, the peak width at half height of that of CC, which indicate the aromatic carbons, decreases obviously during pyrolysis. This means that there is probably only a type of aromatic carbon in NCC play an important role to form the coke, and the condensed degree of these aromatic nucleuses are seldom changed during pyrolysis. In contrast, the aromatic nucleuses of CC are further condensed due to pyrolysis. The main peak of XPS spectra of CC thus gets thinner. Because of the highly condensed aromatic nucleuses or layers, the mechanical strength of the coke formed by CC is usually much higher than that from NCC.

2.3.4. Raman analysis

Fig. 2.15 shows the Raman spectra from NCC and CC, and compares those from sequences of spectrum deconvolution and synthesis. The details of description and definition can be seen in **Table 2.3** and **Section 2.2.3**. While 8 bands have been used in curve-fitting the spectra, there are only 6 main bands for all the samples: G, G_R, V_L, V_R, D and S bands. The rest of bands (G_L, S_L, S_R, and R) virtually represent the curve-fitting residuals. **Fig. 2.15** shows different intensities between the raw coal of NCC and CC. The Raman signals of sp^2 carbons have generally higher intensity than that of sp^3 carbons. The Raman intensity of sp^2 bands can be also enhanced by the conjugation of other sp^2 bonds [28]. CC has higher aromaticity than that of NCC in the raw coals [**Section 2.3.1**], which results in higher Raman intensity of CC. During the pyrolysis, Raman intensities of both the two types of coal will decrease largely. Even through the aromatization during the pyrolysis increases the Raman scattering ability of char by increasing the number of sp^2 carbons, there is another opposite effect on the observed Raman intensity, i.e., the aromatization of char, which also increases the light absorbing ability of char. It is obvious that the increases in the light absorptivity in char seems to be the dominant factor influencing the observed Raman intensity.

The resulting area ratios of different bands are presented in **Fig. 2.16**. The S band can be considered as a brief measure of cross-linking density and substituents. The results show that the ratio of the S peak area to total peak area decreases with increasing pyrolysis temperature for both

the NCC and CC. This means substituents removal during the pyrolysis. The G peak shows the graphitic structure of the coal or coke matrix. The ratio of G peak area to the total, as expected, increases, and this trend is consistent with the results from the NMR, which showed the degree of aromatic-ring condensation increased during the pyrolysis of both NCC and CC. It was also expected that G to D peak area ratio increased monotonously with the pyrolysis temperature, but was not the case. D band exists at the shift ranging from 1344 cm^{-1} to 1382 cm^{-1} in the Raman spectra of this study. According to the Raman spectra of some model aromatic compounds observed by *X. Li et al.* [22], as shown in **Fig. 2.17**, compounds such as naphthalene, benzo-pyrene, and benzo-perylene will have peaks at the range. This indicates that the high carbonated structures (but not definitely same as graphite structure) still cause D peaks. It seems that this effect resulting in increase of D peak area is significant, which is much larger than the effect caused by graphitic structures resulting in the increase of G peak area. Therefore, the peak area ratio (G/D) decreases (as shown in **Fig. 2.16**), especially for NCC. This discovery also explains the fact that NCC, as a non-caking coal, doesn't have a high tensile strength after the pyrolysis, although it has a similar average aromaticity and condensation degree with CC (discussed in **Section 2.3.1**). The key point is that NCC contains of more un-graphitic structures which plays an important role in char property.

2.4. Conclusion

Chemical structures of CC, NCC and their cokes were evaluated by solid state ^{13}C-NMR, FT-IR, XPS and Raman. It was found that CC has less substituents, but higher aromaticity and condensation degree than those of NCC. During pyrolysis, NCC has to be deprived more substituents and produces more gases than CC to evolve an aromatic structure similar to CC. Eventually, it has been impossible to distinguish the coking products of NCC and CC in terms of both aromaticity and condensation degree. Compared with CC, NCC contained more O-containing functional groups, in particular hydroxyl and ester, which were related to the cross-linking reactions during the pyrolysis. It was also found that those reactions related to O-containing groups mainly occur before 500 ℃.

2.5. References

1. Howard JB. *Fundamentals of coal pyrolysis and hydropyrolysis. In: Elliott MA, editor. Chemistry of coal utilization*, New York: Willey, 1981.
2. D. E. Axelson, *Solid State Nuclear Magnetic Resonance of Fossil Fuels; Multiscience: Montreal*, Canada, 1985.
3. S. R. Hartmann, E. L. Hahn, *Phys. Rev.*, 1962, **128**, 2042-2053.
4. J. Schaefer, E. O. Stejskal, R. Buchdahl, *Macromolecules*, 1975, **8**, 291-296.

5. D. L. VanderHart, H. L. Retcofsky, *Fuel*, 1976, **55**, 202-204.
6. V. J. Bartuska, G. E. Maciel, J. Schaefer, E. O. Stejskal, *Fuel*, 1977, **56**, 354-357.
7. R. J. Boucher, G. Standen, R. L. Patience, G. Eglinton, *Org. Geochem*., 1990, **16**, 951-958.
8. M. A. Wilson, E. L. Fargue, D. Gizachew, *APEA J.*, 1994, 210-215.
9. Z. Wang, K. Cheng, C. Zhao, Q. Lu, *Chin. Sci. Bull*., 1997, **42**(6), 478-481.
10. Y. Ge ĺinas, J. A. Baldock, J. I. Hedges, *Org. Geochem*., 2001, **32**, 677-693.
11. D. W. Kuehn, R. W. Snyder, A. Davis, P. C. Painter, *Fuel*, 1982, **61**, 682-694.
12. B. Riesser, M. Starsinic, E. Squires, A. Davis, P. C. Painter, *Fuel*, 1984, **63**, 1253-1261.
13. K, Nishimiya, T. Hata, Y. Imamura, S. Ishihara, *J. Wood Sci*., 1998, **44**(1), 56-61.
14. Z. M. Wang, H. Kanoh, K. Kaneko, G. Q. Lu, D. Do, *Carbon*, 2002, **40**(8), 1231-1239.
15. W. Suliman, J. B. Harsh, N. I. Abu-Lail, A. M. Fortuna, I. Dallmeyer, M. GarciaPerez, *Biomass Bioenergy*, 2016, **85**, 1-11.
16. S. R. Kelemen, P. J. Kwiatek, *Energy Fuels*, 1996, **9**, 841-848.
17. M. Asadullah, S. Zhang, Z. H. Min, P. Yimsiri, C. Z. Li, *Bioresource Technol.*, 2010, **101**, 7935-7943.
18. A. Cuesta, P. Dhamelincourt, *Carbon*, 1994, 32, 1523-1532.
19. M. S. Solum, R. J. Pugmire, D. M. Grant, *Energy Fuels*, 1989, **3**, 187-193.
20. S. R. Kelemen, M. Afeworki, M. L. Gorbaty, *Energy Fuels*, 2002, **16**, 1450-1462.
21. X. J. Li, J. I. Hayashi, C. Z. Li, *Fuel*, 2006, **85**, 1509-1517.
22. X. J. Li, J. I. Hayashi, C. Z. Li, *Fuel*, 2006, **85**, 1700-1707.
23. K. Kidena, S. Murata, L. Artok, M. Nomura, *Jpn. Inst. Energy*, 1999, **78**, 869-876.
24. T. H. Fletcher, M. S. Solum, D. M. Grant, S. Critchfield, R. J. Pugmire, *Twenty-Third Symposium (International) on Combustion/The Combustion Institute*, 1990, 1231-1237.
25. L. Qian, S. Z. Sun, D. Wang, H. R. Guo, H. H. Xu, J. Q. Meng, Y. K. Qin, *J. Chi. Coal Soci*., 2013, **38**(3), 455-460.
26. L. Liu, Y. Cao, Q. C. Liu, *Fuel*, 2015, **146**, 103–110.
27. B. Shokri, M. A. Firouziah, S. I. Hosseini, *Proceedings of 19th international symposium on plasma chemistry society*. 2009, **2631**.
28. L. A. Leites, S. S. Bukalov, *J. Raman Spectrosc.*, 2001, **32**, 413-424.

Table 2.1. Elementary analysis of NCC, CC, and their cokes (wt%-dry coal).

Coal	Heat treated	Yield, [g/g-dry coal]	H	C	N
NCC	Raw	-	5.2	70.0	0.9
	400 ℃	0.86	4.6	73.8	1.0
	450 ℃	0.73	4.2	75.2	1.0
	500 ℃	0.69	3.5	77.8	1.1
	600 ℃	0.63	2.9	82.6	1.2
	700 ℃	0.56	2.2	89.3	1.2
CC	Raw	-	4.6	80.9	1.8
	400 ℃	0.98	4.5	80.8	1.8
	450 ℃	0.95	4.4	80.7	1.8
	500 ℃	0.91	4.0	81.2	1.9
	600 ℃	0.84	3.0	81.5	2.0
	700 ℃	0.81	2.1	83.4	2.0

Table 2.2. Determination of ^{13}C-NMR curve fitting (ppm).

	CH_3	CH_2	Al-O	Ar-H	Bridgehead	Ar-C	Ar-O	COO, C=O
Peak position	13, 20	31, 40	56, 73, 93	103, 113	126	140	153, 167	178, 187
HW	10~12	6~13, 16~17	16~18	17~18	17~18	16~17	15~16	12~15

Al: aliphatic carbon, Ar: aromatic carbon, Bridgehead: bridgehead and internal aromatic carbon,

HW: Half Width.

Table 2.3. Summary of peak/band assignment.

Band name	Band center, cm^{-1}	Description
G_L	1700	Carbonyl group C=O
G	1598	Graphite E^2_{2g}; aromatic ring quadrant breathing
G_R	1540	Amorphous carbon structures
V_L	1480	Methylene or methyl; semi-circle breathing of aromatic rings; amorphous carbon structures
V_R	1440	Methylene or methyl; semi-circle breathing of aromatic rings; amorphous carbon structures
D	1360	D band on highly ordered carbonaceous materials; C-C between aromatic rings
S_L	1310	Aryl-alkyl ether; para-aromatics
S	1240	$C_{aromatic}$-C_{alkyl}; aromatic (aliphatic) ethers; C-C on hydro-aromatic rings; C-H on aromatic rings

G: graphite; G_R: G right; G_L: G left; V_R: valley right; V_L: valley left; D: defect;

S: on the side of the D band; S_R: S right.

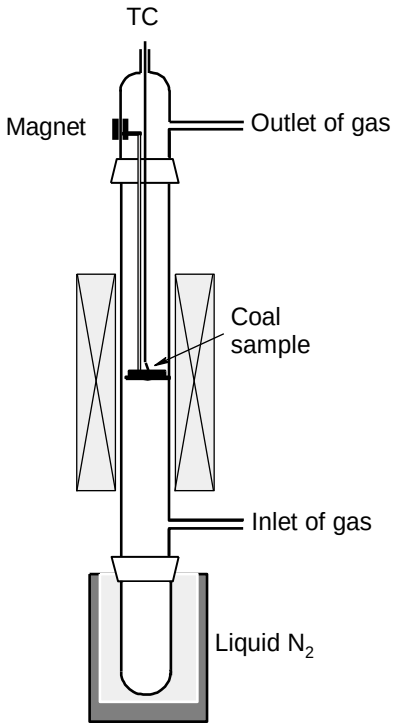

Fig. 2.1. Apparatus of tube reactor for cokes.

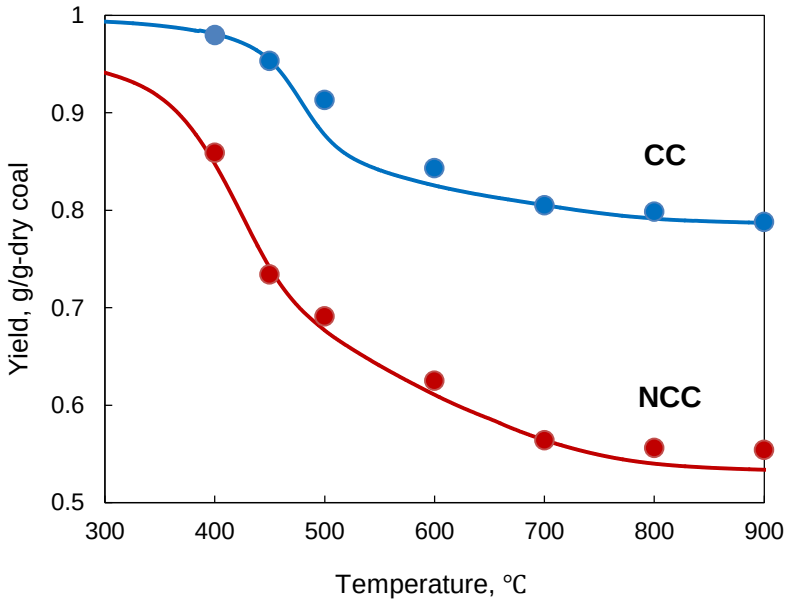

Fig. 2.2. Yields of heat treatment coals (plots) and TG curves of CC and NCC.

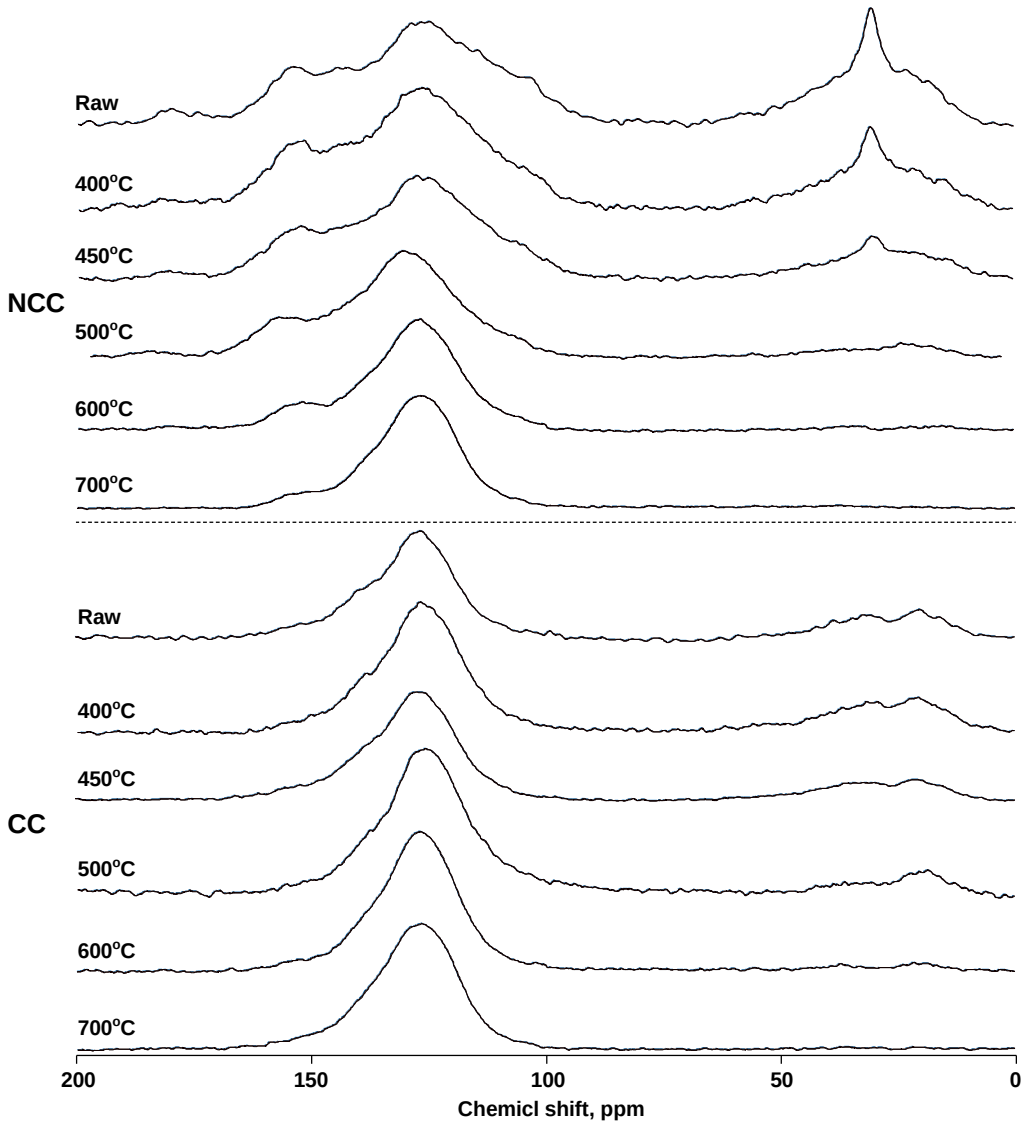

Fig. 2.3. ^{13}C-NMR spectrum of NCC, CC, and their cokes.

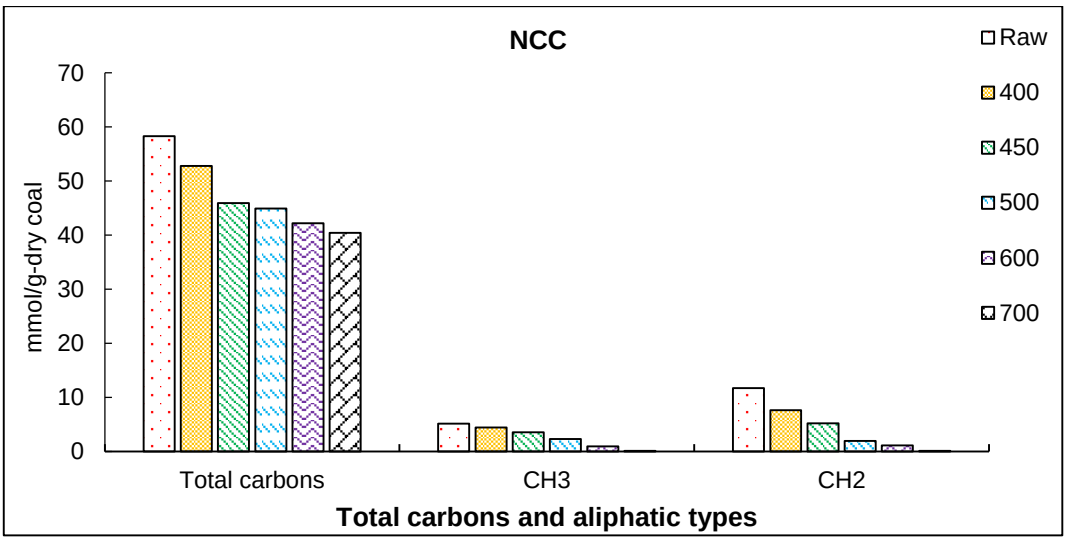

Fig. 2.4. Aliphatic carbon structural distribution of NCC and its cokes.

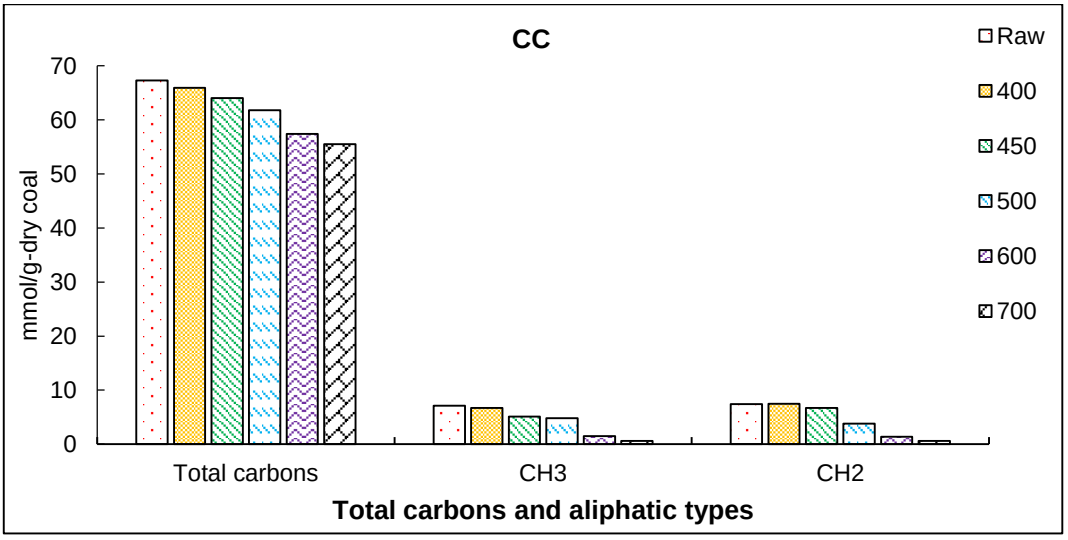

Fig. 2.5. Aliphatic carbon structural distribution of CC and its cokes.

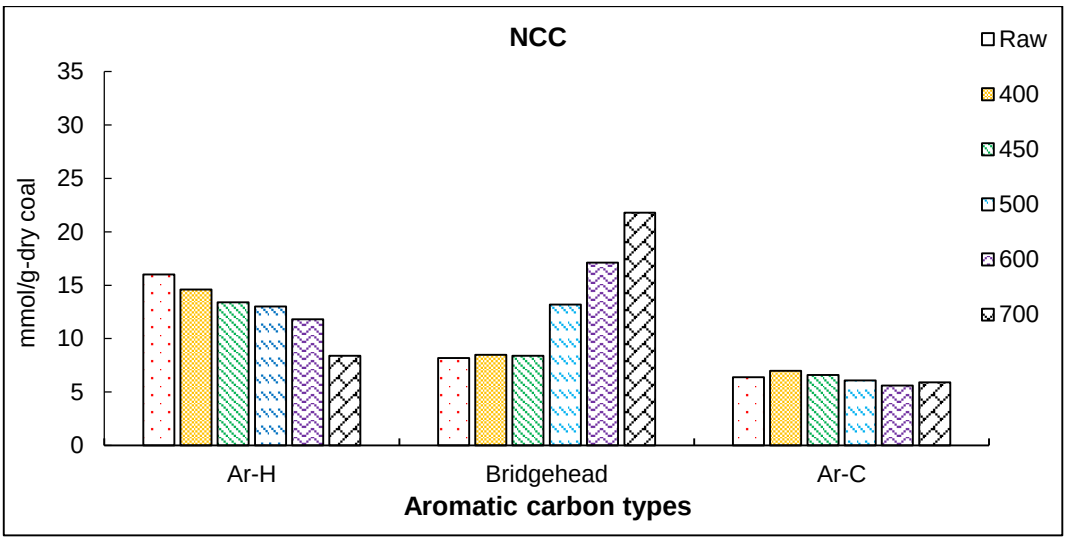

Fig. 2.6. Aromatic carbon structural distribution of NCC and its cokes.

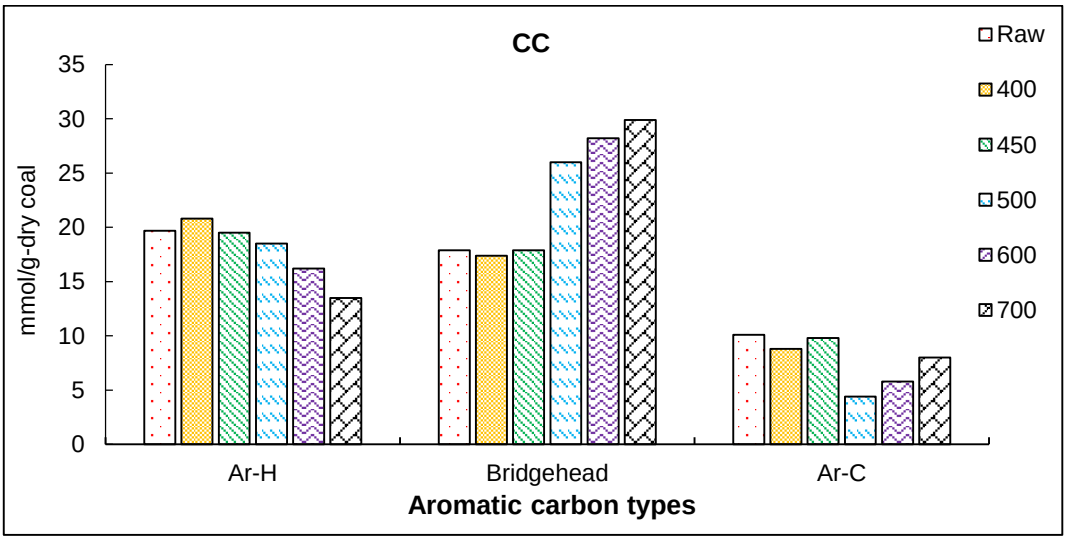

Fig. 2.7. Aromatic carbon structural distribution of CC and its cokes.

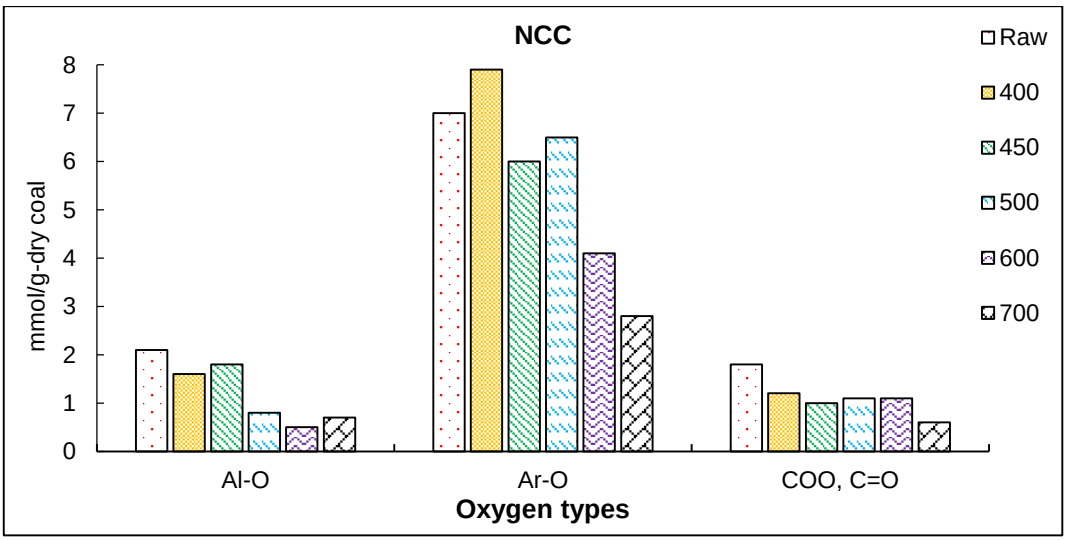

Fig. 2.8. Structural distribution of carbons associated with oxygen in NCC and its cokes.

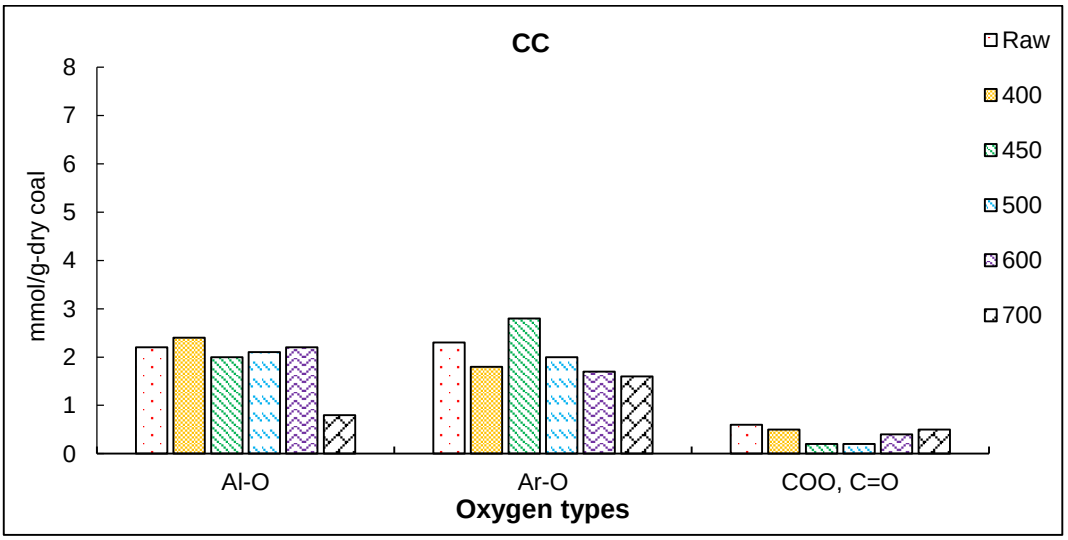

Fig. 2.9. Structural distribution of carbons associated with oxygen in CC and its cokes.

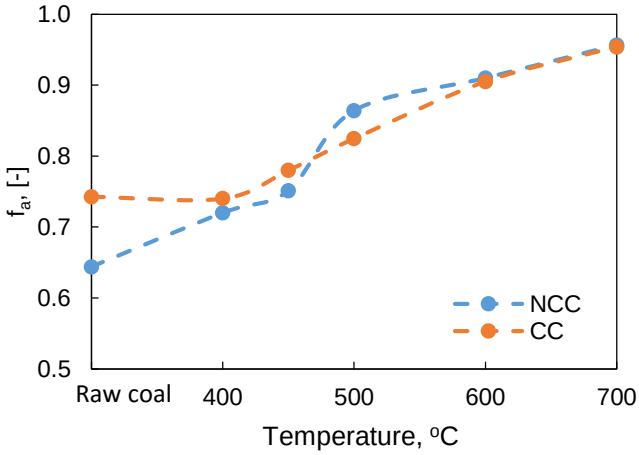

Fig. 2.10. Aromaticity (f_a)as a function of temperature for NCC and CC.

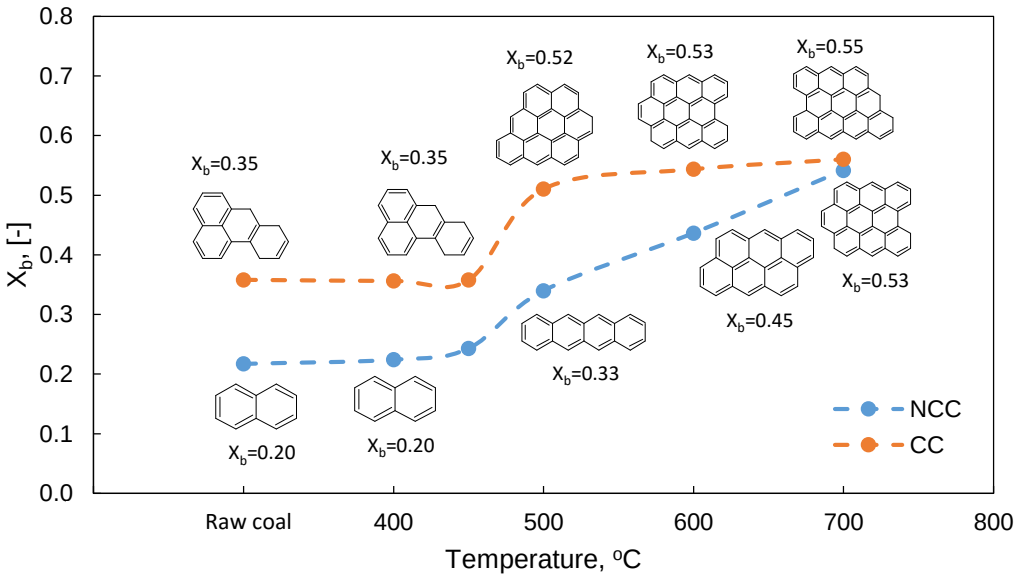

Fig. 2.11. Aromatic condensation degree (X_b) as a function of temperature for NCC and CC.

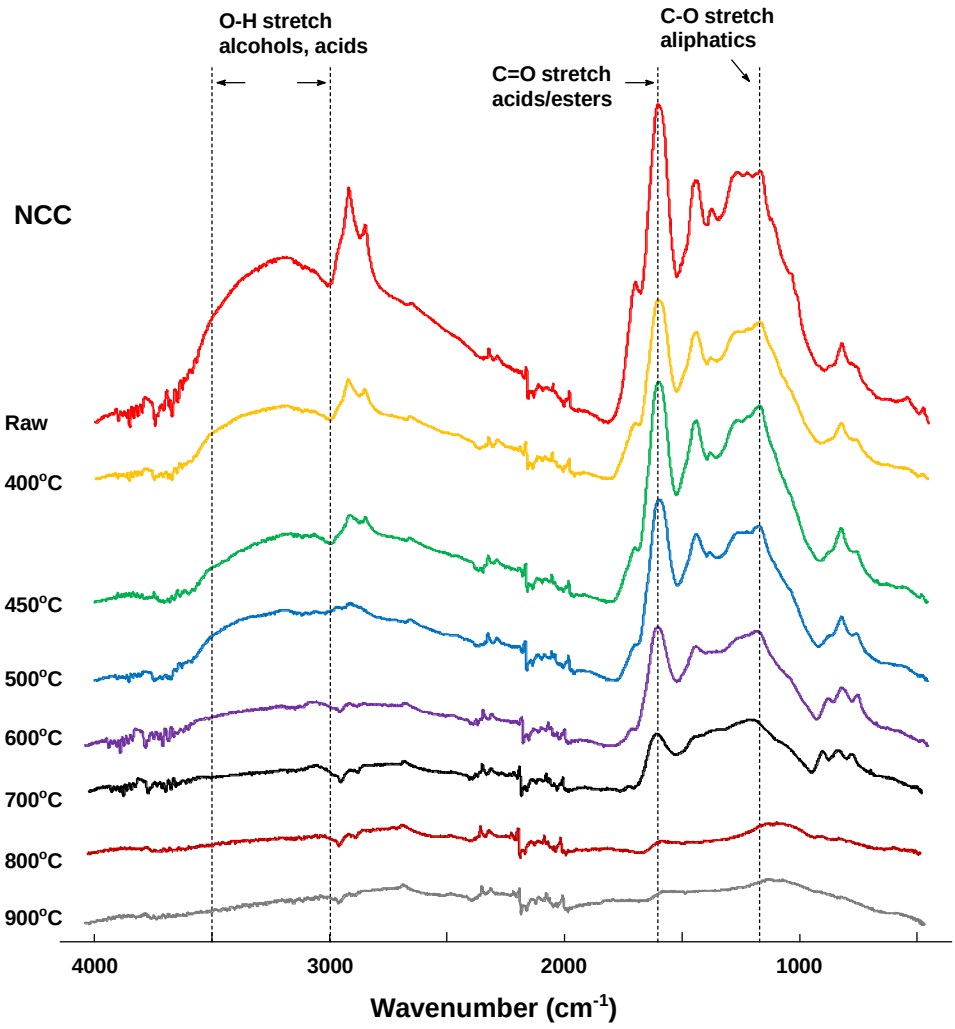

Fig. 2.12. FT-IR spectrogram of NCC and its cokes.

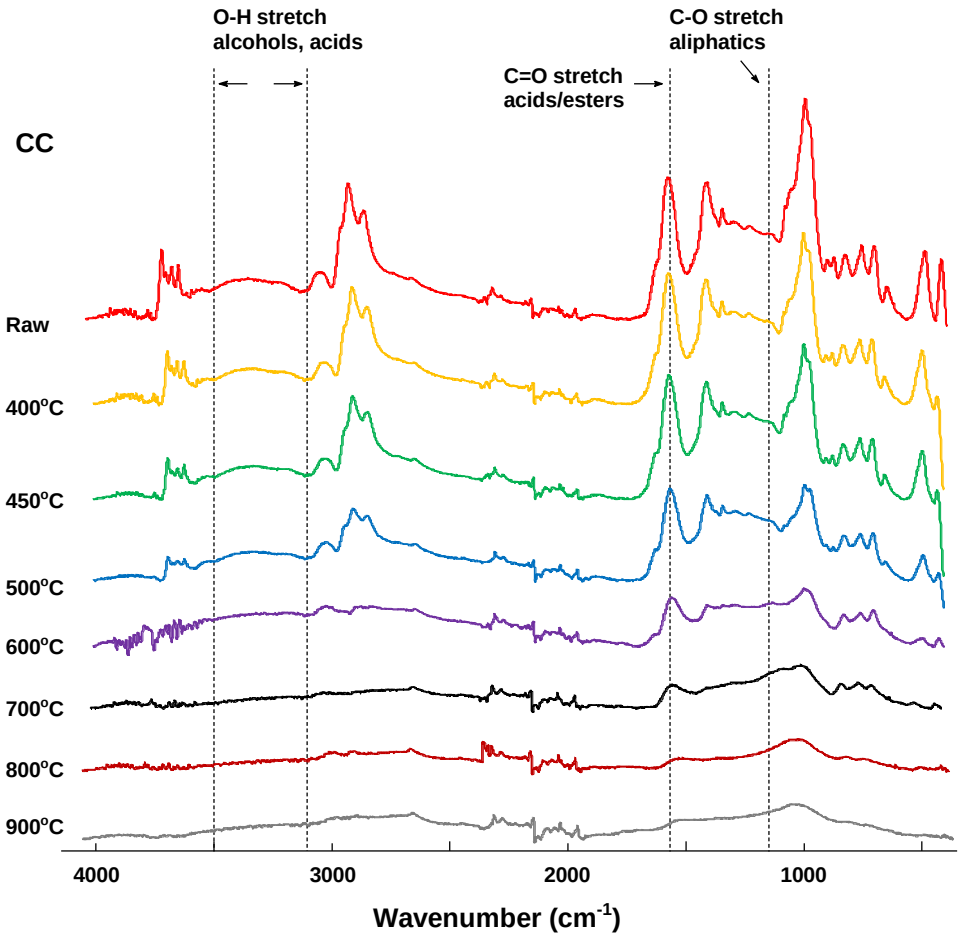

Fig. 2.13. FT-IR spectrogram of CC and its cokes.

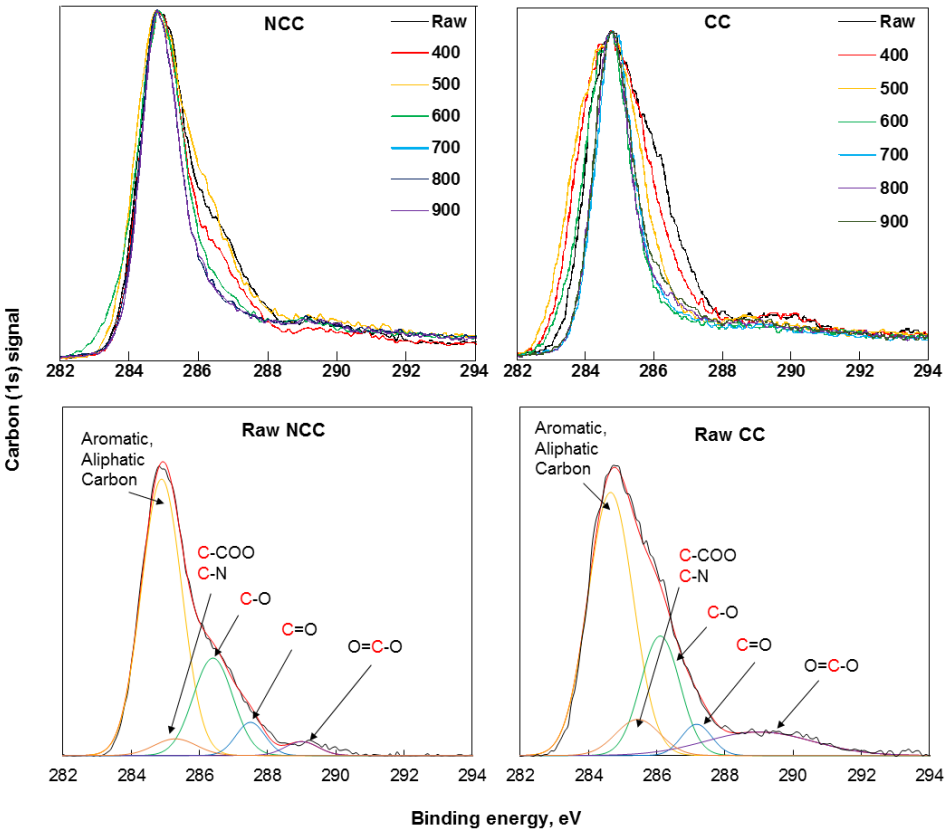

Fig. 2.14. XPS spectra and the assignments of deconvoluted peaks of NCC, CC, and their cokes.

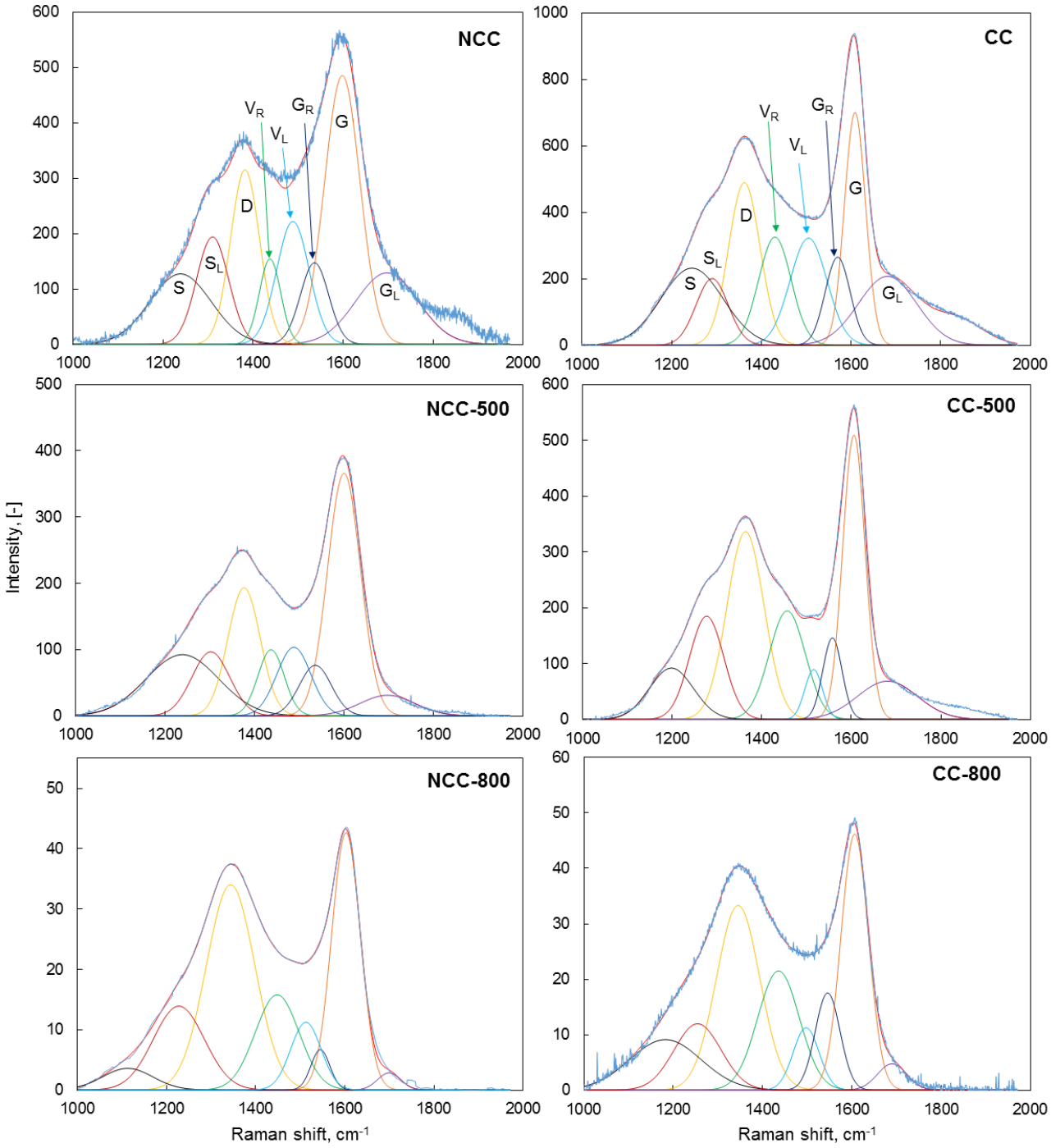

Fig. 2.15. Deconvolutions of Raman spectrum of NCC, CC, and their cokes at 500 and 800 ℃.

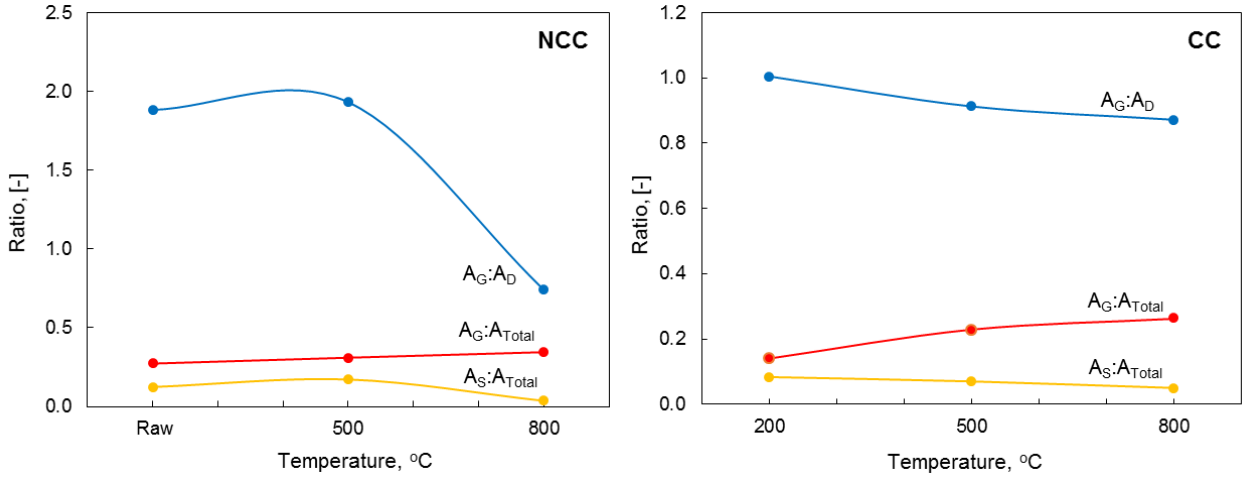

Fig. 2.16. Area ratios of different band of NCC, CC and their cokes at 500 and 800 ℃.

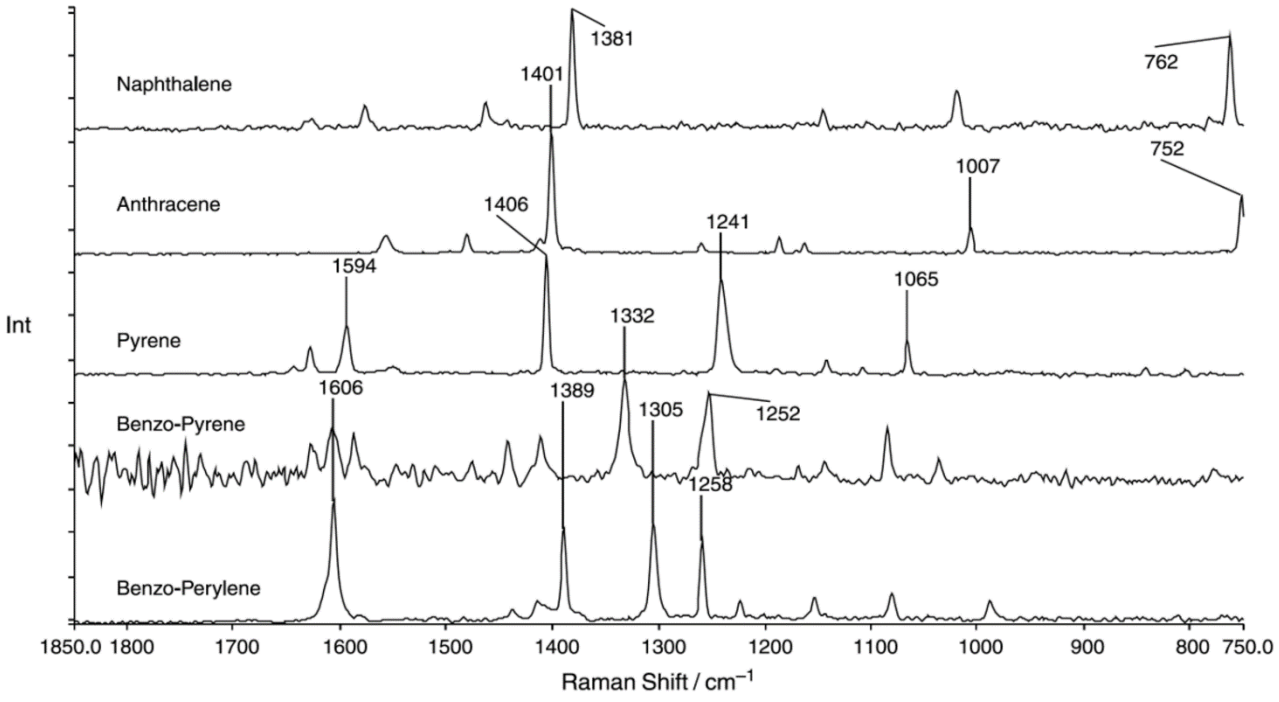

Fig. 2.17. Raman spectra of model aromatic compounds. (*X. J. Li et al, Fuel, 2006, 85*)

Chapter 3

Characteristics of gas evolution profiles during coal pyrolysis and its relationship with the variation of functional groups

3.1. Introduction

It is generally recognized that the heterogeneous structure of coal is formed by a complex three-dimensional macromolecular network cross-linked by short aliphatic and etheric bridges [1]. A variety of substituents, such as hydroxyl, ether, ester, carboxyl, and alkyl groups are attached to the discrete/condensed aromatic rings in coal to form the main structure of coal macromolecules [2,3]. Pyrolysis is a most generally used technology for down-stream processing and clean utilizations of coal [4]. With the thermal decomposition of coal macromolecules, the substituents on the aromatic rings, including side substituents and bridged ones, are gradually deprived by the release of micro-molecules, e.g., H_2, CH_4, H_2O, CO, CO_2, etc. [5]. The relationships between substituents on aromatic rings and the volatile products have been extensively studied, but only qualitatively and superficially [6-10]. For example, there were report indicating that methyl groups can be deprived and then capped by a hydrogen-free radical to form a methane at high temperature, while other reports concluded that at moderate temperatures the methane formation occurred as well even at moderate temperature, caused by cross-linking reactions. Therefore, mechanisms of the formation of volatile products in coal pyrolysis still remains inconsistent and elusive, even though new reaction models for coal pyrolysis have been proposed in recent years [7,11-21].

To study the strict relations between the deprivations of substituents on aromatic rings in coal and the formation of volatile products in coal pyrolysis, the volatile products were always qualitatively or quantitatively analyzed by employing a variety of techniques, such as quadrupole mass spectrometry (QMS), Fourier transform infrared spectroscopy (FT-IR), and gas chromatography (GC) [21,22]. Many studies have successfully employed QMS and FT-IR for real-time detecting the pyrolysis behavior of coal and its gaseous compounds evolution due to the rapid response and sensitivities of QMS and FT-IR [23-27]. FT-IR is, however, not as sensitive as QMS for those micro-molecules in the volatile products. Moreover, QMS and FT-IR are always employed for qualitative analysis rather than quantitative one [28]. Compared with QMS and FT-IR, GC operation is more accurate and reliable for quantitative analysis, but it has always to be off-line performed for compromising its defect of batch sampling. In addition, nuclear magnetic resonance (NMR) spectroscopy can provide powerful structure information on the different kinds of organic carbons, hydrogens, and oxygen-containing groups in coal, and additionally has good quantitative properties. The solid-state ^{13}C

NMR spectroscopy has been widely applied to directly characterize the carbon structural features and functional groups in fossil fuel in the past several decades [29-35].

In this study, real-time measurements by QMS combined with off-line analysis by GC were performed qualitatively and quantitatively to analyze the evolution rate of each gas along with the pyrolysis of caking coal and non-caking coal. ^{13}C NMR was performed to identify the structural information and the variety of organic carbons in raw coals and the corresponding staged char residues from the coal pyrolysis [36]. Based on a famous coal model FG/DVC created by Solomon et al. [37], we analyzed these data or information gotten from QMS, GC, and ^{13}C NMR systematically, and then presented the relationships between the substituents on aromatic rings in coal and the evolution products, as well as the potential mechanisms of gas formation during coal pyrolysis.

3.2. Experimental section

3.2.1. Samples

Caking coal (CC) and non-caking coal (NCC) were used in this study. The proximate and ultimate analyses are listed in **Table 3.1**. The coal samples were pulverized to less than 75 μm and dried under vacuum for 24 h.

3.2.2. Coal pyrolysis and analysis to the gas products

Coal powders of 2.0 g were used in each experiment. As shown in **Fig. 3.1**, loose-packed coal powders were heated up to 900 ℃ with a heating rate of 5 ℃/min in a horizontal quartz tube reactor, with using argon as carrier gas with a constant flow rate of 200 ml/min (STP). Filtrated by quartz wool at the tail end of the quartz tube reactor, the volatile products from coal pyrolysis were detected by only one of two separated modes, QMS or GC.

QMS (M-QA100TS, ANELVA Corp.) was used for real-time monitoring. The volatile products were introduced into the QMS through a capillary, which was convolved by tape heater of 200 ℃ to avoid condensation of coal tar therein. A diaphragm pump was used to help transporting the gas into the QMS by reducing the tube pressure to 25 mbar. The delay time of QMS detection was thus decreased within 5 s. The vacuum degree of QMS was kept at 1×10^{-5} Pa before measurement, and at 1×10^{-3} Pa during measurement. Other details of QMS operation were set as follows: ionizing voltage, 24 V; emission current, 1.0 mA; mass number range, 1−80 m/z; scan speed, 100 ms/amu. Mass numbers of 2, 15, 18, 28, and 44 were selected to characterize the presences of H_2, CH_4, H_2O, CO, and CO_2, respectively. Real-time evolution curves of these five gases during coal pyrolysis were thus obtained.

GC-TCD/FID (Himadzu, GC-8A and GC-14B) was used for off-line detection. Sufficiently cooled in two cold traps (0 ℃ and −70 ℃), the non-condensable volatiles were collected into a gas bag, and then analyzed by GC-TCD/FID. H_2O in coal tar, which had been retained by the quartz wool in tube reactor and the cold traps, was analyzed by Karl Fischer Moisture analyzer (MKC-210, KYOTO ELECTRONICS). Distribution of products from coal pyrolysis is shown in **Table 3.2**. The data that were obtained from off-line GC assisted the quantitative analysis of the evolution curves of gas products that were obtained from real-time QMS. Therefore, the function curves of gases production during coal pyrolysis with variables of temperatures were finally obtained by employing differential method.

Coal powders were further briquetted at ambient temperature and with mechanical pressure of 128 MPa for 8 min. Each briquette (1.0 g) was heated up to different target temperatures at the same heating rate of 5 ℃/min with a N_2 flowrate of 200 ml/min (STP) in a vertical quartz tube reactor for heat treatment coals, as shown in **Fig. 2.1**. Once reaching the target temperatures, the char briquettes were instantaneously cooled down by falling into the bottom of the reactor immersed in liquid N_2. Yields of heat treatment coals at different temperatures are shown in **Fig. 2.2**. Thermo-gravimetric (TG) curves of the two coal samples were presented in that figure as well. Note that the TG curves are well consistent with those dots of yields, indicating the accuracy of our experiments. Residual heat treatment coals were then pulverized to powders for the characterizations by solid-state ^{13}C NMR spectroscopy. The NMR spectra were recorded with the DEPTH2 technique at 100.53 MHz in a JEOL ECA 400 spectrometer. The repetition time was 20 s. Magic angle spinning was performed at 15 kHz in the commercial probe (JEOL 4 mm CPMAS). The ^{13}C NMR data were then analyzed by a variation of the method described by Solum et al. [36].

3.3. Results and discussion

In our study, all the evolution curves of gases formation were deconvoluted by several independent Gaussian-style functions, varying their parameters such as the locations, line widths, and intensities, to get the highest correlation coefficients. All the correlation coefficients of deconvolution results were higher than 99%. ^{13}C NMR spectra were deconvoluted based on the chemical shifts in previous reports [36,38], analyzing the organic carbon varieties in the molecules of coal samples. With the help of elemental analysis of raw coal (**Table 3.1**), the organic carbons can be quantitatively classified into 8 varieties, i.e., methyl (CH_3), methylene (CH_2), aliphatic carbon with oxygen substituents (Al-O), protonated aromatic carbon (Ar-H), aromatic carbon with alkyl groups (Ar-C), bridgehead carbon, aromatic carbon with oxygen substituents (Ar-O), and carbonyl carbon (O=C-O, C=O) (see **Table 3.3** and **3.4**). CH_4, CO_2, CO, H_2O, and H_2 are the main gas products from

coal pyrolysis, and these gases are relative with specific functional groups of coal [7,39-41], therefore, it is evident to quantitatively associate the gas outputs with the quantities of the functional groups.

3.3.1. Mechanism of CO formation

Fig. 3.2 shows the yields of CO with elevated temperatures of coal pyrolysis, and the variations of the related Al-O and Ar-O. With the temperature elevated, CO formation is continuously increased, while the quantities of the two kinds of functional group Al-O and Ar-O are not linearly changed.

I. Ar-O increases while Al-O slightly decreased before 400 ℃. It was because the side carbon chains in coal transformed into aliphatic carbon rings, and ether bonds were dissociated at the relative low temperature range. To be specific, coking process at low temperatures during coal pyrolysis resulted in the ring formation of side carbon chains. When a side carbon chains contained a primary hydroxyl group originally, the ring formation would cause the formation of Ar-O bonds (Reaction 1). Ether bonds were also easy to be dissociated during coal pyrolysis at low temperature, producing CO gas or carbonyl group, which should be the reason for the quantity of Al-O decreasing (Reaction 2). In the reactions, (coal)Ar- denotes the layer structure of aromatic rings in coal, while R- represents the substituents such as alkyl groups or aromatic rings.

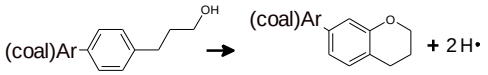

(1)

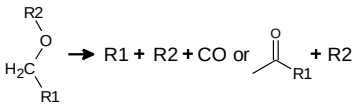

(2)

II. At the temperature range from 400 to 450 ℃, the quantity of Ar-O decreased greatly while that of Al-O elevated slightly. In this stage, the formation of CO was not only related to Reaction 2, but also with Reaction 3. As shown in Reaction 3, the carbonyl group will be generated from the cleavage of Ar-O bond of Ar-O-R, only if -R denotes long-chain alkyl groups. CO is also possible to be formed only if -R represents -CH_3. In addition, Al-O slightly increasing at the temperature range was probably attributed to the transferred ether groups from aromatic rings to side chains (see Reaction 4).

(3)

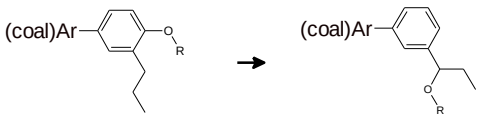

(4)

III. At the temperature range from 400 to 450 ℃, Ar-O increases while Al-O deceases. In this stage, the formation of CO was still attributed to Reaction 2 and 3. In addition, other reactions such

as the condensation between O-containing heterocyclic compounds and aromatic rings, and aromatization of cycloalkanes should occur in this stage. Both of these two reactions can increase the quantity of Ar-O (Reaction 5 and 6). Moreover, according to these two reactions, the quantity of bridgehead C atoms should be increased simultaneously, which is also verified by the NCC profile in **Fig. 3.3**.

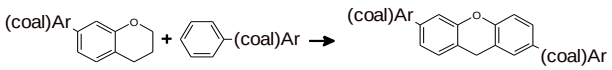

(5)

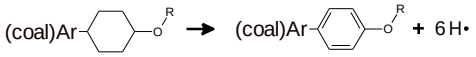

(6)

IV. At the temperature range from 500 to 600 ℃, the quantity of Ar-O begins decreasing significantly, while that of Al-O is continuously decreasing. In this stage, there was still CO gas generated through Reaction 2 and 3. Meanwhile, with deprivation of O atoms to form oxygen free radicals and to produce CO eventually, the O-containing aromatic rings started to condense, forming bigger condensed arenes. As a result, the quantity of Ar-O decreased largely.

V. Above 600 ℃, Ar-O decreases continuously due to the presence of Reaction 7, while Al-O increased slightly since a few oxygen free radicals reacted with the side substituents of aromatic rings (Reaction 8).

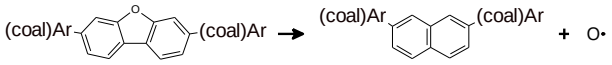

(7)

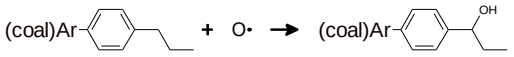

(8)

As shown in **Table 3.3** and **3.4**, and **Fig. 3.4**, compared with NCC, CC contains similar amount of Al-O but less Ar-O, while the CO formation of CC is less than that of NCC. This further verifies that the formation of CO is closely relative with Ar-O. It is interesting that the variation profiles of Ar-O and Al-O of CC at the temperature range from ambient to 600 ℃ are similar with those of NCC at the temperature range from 400 to 700 ℃. This phenomenon implies that the molecular structures of CC might be similar with those of NCC after treatment of pyrolysis at low temperatures. From ambient temperature to 600 ℃, the Ar-O in CC should react successively as Reactions from 3 to 7, while Al-O should react as Reaction 2, 6, and 8. When the temperature was elevated above 600 ℃, the quantity of Ar-O remained unchanged, while Al-O decreased greatly to form CO gas. This was mainly because the further pyrolysis of side substituents on aromatic rings occurred as Reaction 8.

According to the above-mentioned analysis about the CO formation and the variations of related functional groups, we deconvoluted the CO formation rate profiles of CC and NCC, and further identified each independent reaction we proposed. According to previous reports, the CO formation of coal pyrolysis was closely related to three to five potential reactions [42-44]. As shown in **Fig. 3.5**

(a) and **(b)**, and **Table 3.5**, we recognize that the CO formation is attributed to four independent reactions (correlation coefficients are higher than 99%). CO formation at low temperatures was related to the cleavage of ether group (Reaction 2), and this reaction occurred at a relative wide temperature range from 300 to 500 ℃ [1]. Peak 1 is thus assigned to Reaction 2. The reaction indicated by Peak 2 should be caused by the pyrolysis of anhydrides, which forms CO and CO_2 at *ca.* 600 ℃ [45,46]. Note that parts of these anhydrides existed originally in the raw coals, while other parts should come from the condensation of -COOH groups simultaneous with the H_2O formation. Peak 3 was relative with the cleavage of carbonyls, which can produce CO at a high temperature [39]. Peak 4 can be assigned to free radical reactions. As above mentioned, the quantity of Ar-O started decreasing greatly since 500 ℃, meanwhile the further condensation among aromatic rings were initiated. The condensation processes removed the O atoms, which then reacted with C and H atoms easily to form CO and H_2O, respectively.

The reactions involving oxygen free radicals were the main sources of CO formation both for NCC and for CC, while one of the CO sources of CC at low temperature, the cleavage of ether groups, was not as significant as that of NCC. This means the ether groups should widespread in non-caking coal.

3.3.2. Mechanism of CO_2 formation

The deconvolution results of rate profiles of CO_2 formation are shown in **Fig. 3.5 (c)** and **(d)**, in which Peak 1 is located at low temperature, and Peak 2 and 3 are located at 400 and 600 ℃. These three peaks were attributed to the removal of carboxyl, ester group, and anhydride, respectively [47-50]. Note that, according to previous studies, the Peak 3 might include a few contributions from the decomposition of mineral substances at the temperature range from 600 to 700 ℃ [51,52], otherwise the quantity of CO_2 formed at this temperature range should be same with that of CO (see Peak 2 of **Table 3.5**, a and b) since the decomposition of anhydrides could generate same amount of CO_2 and CO.

In **Table 3.5**, the quantities of CO_2 of NCC and CC are so different that CO_2 formation of NCC (1.72 mmol) is 15 times as much as that of CC (0.11 mmol). This was mainly caused by the different quantities of COO and C=O groups in NCC and CC. There was 1.8 mmol COO and C=O in NCC, while that in CC was only 0.6 mmol.

3.3.3. Mechanism of CH_4 formation

The formation of CH_4 was related to the cleavage of $-CH_3$. As shown in **Fig. 3.6** and **3.7**, with increasing the temperature, the amount of $-CH_3$ decreases gradually, and the CH_4 is produced

continuously. There were several -CH_3 types in coal, and the removals of different -CH_3 groups occurred at different temperature ranges. The -CH_3 attached to the aromatic rings in coal molecules can be classified into three groups in addition to those bonding with heteroatoms (see **Fig. 3.8**). However, these -CH_3 types cannot be distinguished from each other through ^{13}C NMR spectra.

As shown in **Fig. 3.5 (e)** and **(f)**, the formation of CH_4 can be attributed to three independent reactions. At the temperature range from 400 to 700 ℃, the CH_4 should be generated from the cleavage of β-CH_3 (-$^1CH_3$ in **Fig. 3.8**). When the temperature was elevated to 600 ℃, the cleavage of Ar-CH_3 occurred (-$^2CH_3$ in **Fig. 3.8**). The formation of CH_4 at the temperature higher than 600 ℃ should be related to the secondary pyrolysis of the long-chain alkanes attached to aromatic rings, since the pyrolysis of such alkanes required very high energy (-$^3CH_3$ in **Fig. 3.8**). Our study is also supported by previous reports [47,52,53]. Liu [54] proposed the mechanisms of CH_4 formation for coal pyrolysis at the temperature range from 400 to 700 ℃, which is well consistent with our results.

In **Fig. 3.5 (e)** and **(f)**, the temperature range of CH_4 formation of NCC is similar with that of CC. However, compared with NCC, whose β-CH_3 is the main resource for CH_4 formation, the CH_4 produced by CC is mainly generated from the cleavage of Ar-CH_3. This means that there are many bridged alkyls and long side chains in the coal molecules of NCC, while the condensed degree of CC is much higher than that of NCC, such that the alkyls of CC are mainly attached to the aromatic rings.

3.3.4. Mechanism of H_2O formation

As shown in **Fig. 3.9**, the temperature range from ambient to 900 ℃ for H_2O formation is wider than that of any other gases. The physically adsorbed H_2O in coal was emitted when the temperature is lower than 300 ℃, while the pyrolysis of coal (mainly as the cleavage of –OH groups) at the temperature higher than 300 ℃ became the main resource of H_2O formation [6,55]. The formation of H_2O was closely related to so many potential reactions that its temperature range is the widest. It was thus impossible to deconvolute its formation profile exactly. For example, as seen in Reactions 9 to 11, the cleavage of -OH was an important source for H_2O formation, while other groups such as ether, ester, and anhydride that underwent pyrolysis at high temperature would produce oxygen free radicals to generate H_2O eventually as well.

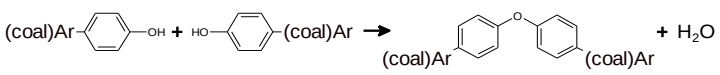

(9)

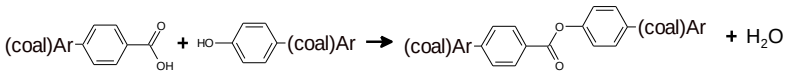

(10)

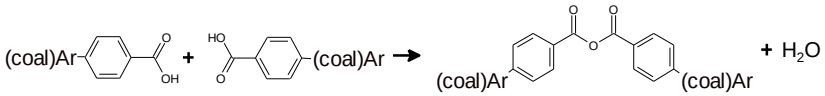

(11)

3.4. Conclusions

Based on the QMS analysis of the product gases of CC and NCC and the ^{13}C NMR spectra, the mechanism of coal structure changes at molecular level during pyrolysis are quantitatively revealed.

1) The CO formation can be mainly attributed to the cleavage of ether group, the removal of anhydrides, oxygen free radicals reaction, and cleavage of carbonyl groups. The removals of carboxyl, ester, and anhydride groups are the main reasons for the CO_2 formation.
2) The quantity of Ar-O during coal pyrolysis will temporarily increase during coal pyrolysis due to the secondary effects of some reactions such as cyclization of side chains containing hydroxyl groups and condensation of O-containing aromatics. The quantity of Al-O increases temporarily as well, because of the migration of O free radicals.
3) The formation of H_2O must be followed by those of CO and CO_2. With the formation of anhydrides, esters, and ethers, the reactions among different carboxyl and hydroxyl groups during coal pyrolysis generate H_2O first, and then their further reactions of removing anhydrides and esters must cause the formations of CO and CO_2.
4) The formation of CH_4 is relatively independent from that of other volatile products. It is generated by the cleavages of β-CH_3, Ar-CH_3, and long chain alkanes attached to the aromatic rings in coal molecules. The dissociation energies of methyls of different locations are greatly different from each other, so the main temperature ranges for CH_4 formation depend largely on the coal ranks.

In addition, the different performances of coals with different ranks during pyrolysis are ascribed to their different quantities and distributions of O-containing functional groups, alkyls, and scales of aromatic rings. Representing caking coal, CC has less substituents, but higher aromaticity and condensation degree than those of NCC representing non-caking coal.

3.5. References

1. J. X. Liu, X. M. Jiang, J. Shen, H. Zhang, *Energy Convers. Manage.*, 2014, **87**, 1039–1049.
2. F. E. Ndaji, L. M. Butterfield, K. M. Thomas, *Fuel*, 1997, **76**(2), 169–177.
3. M. L. Poutsma, *Energy Fuels*, 1990, **4**(2), 113–131.
4. S. Shabbar, I. Janajreh, *Energy Convers. Manage.*, 2013, **65**, 755–763.
5. A. Arenillas, F. Rubiera, J. J. Pis, *J. Anal. Appl. Pyrolysis*, 1999, **50**, 31–46.
6. J. V. Ibarra, R. Moliner, M. P. Gavilan, *Fuel*, 1991, **70**, 408–413.
7. P. R. Solomon, D. G. Hamblen, R. M. Carangelo, M. A. Serio, G. V. Deshpande, *Energy Fuels*, 1988, **2**, 405–422.
8. A. Attar, G. G. Hendrickson, *Am. Chem. Soc., Div. Fuel Chem., Prepr.*, 1980, **25**(4), 150-160.

9. S. Y. Liu, Z. Q. Zhang, H. F. Wang, *J. Mol. Model*, 2012, **18**, 359–365.
10. P. R. Solomon, D. G. Hamblen, M. A. Serio, Z. Z. Yu, S. Charpenay, *Fuel*, 1993, **72**(4), 469–488.
11. S. Niksa, *Energy Fuels*, 1991, **5**, 647–665.
12. S. Niksa, *Energy Fuels*, 1991, **5**, 665–673.
13. S. Niksa, *Energy Fuels*, 1991, **5**, 673–683.
14. S. Niksa, *Combust. Flame*, 1995, **100**, 384-394.
15. D. M. Grant, R. J. Pugmire, *Energy Fuels*, 1989, **3**, 175-186.
16. T. H. Fletcher, A. R. Kerstein, *Energy Fuels*, 1990, **4**, 54-60.
17. T. H. Fletcher, A. R. Kerstein, *Energy Fuels*, 1992, **6**, 414-431.
18. Y. J. Tian, K. C. Xie, S. Y. Zhu, T. H. Fletcher, *Energy Fuels*, 2001, **15**, 1354-1358.
19. P. R. Solomon, *Twenty-Fifth Symposium (International) on Combustion/The Combustion Institute*, 1994, 463-474.
20. P. R. Solomon, D. G. Hamblen, Z. Z. Yu M. A. Serio, *Fuel*, 1990, **69**, 754-763.
21. P. R. Solomon, M. A. Serio, R. M. Carangelo, R. Bassilakis, *Energy Fuels*, 1990, **4**, 319-333.
22. D. Dollimore, G. A. Gamlen, T. J. Taylor, *Thermochim. Acta*, 1984, **75**, 59-69.
23. D. Wu, G. J. Liu, R. Y. Sun, *Energy Fuels*, 2014, **28**, 3024−3035.
24. S. Q. Wang, Y. G. Tang, H. H. Schobert, Y. N. Guo, W. C. Gao, X. K. Lu, *J. Anal. Appl. Pyrolysis*, 2013, **100**, 75–80.
25. L. Y. Jia, J. J. Weng, Y. Wang, S. B. Sun, Z. Y. Zhou, F. Qi, *Energy Fuels*, 2013, **27**, 694−701.
26. L. Duan, C. S. Zhao, W. Zhou, C. R. Qu, X. P. Chen, *Energy Fuels*, 2009, **23**, 3826–3830.
27. C. L. Duan, *Master dissertation of Taiyuan University of Technology*, 2007.
28. C. D. Le, S. T. Kolaczkowski, D. W. J. McClymont, *Fuel*, 2015, **139**, 337–345.
29. D. E. Axelson, *Multiscience: Montreal, Canada, and CANMET, Canadian Government Publishing Centre, Supply and Services of Canada: Ottawa*, 1985.
30. R. M. Davidson, *London: IEA Coal Research*, 1986.
31. F. P. Miknis, *Annual Reports on NMR Spectroscopy*, 1996, **33**, 207–246.
32. D. Genetti, T. H. Fletcher, R. J. Pugmire, *Energy Fuels*, 1999, **13**, 60-68.
33. S. T. Perry, E. M. Hambly, T. H. Fletcher, M. S. Solum, *R. J. Pugmire, P. Combust. Inst.*, 2000, **28**, 2313–2319.
34. Q. L. Sun, W. Li, H. K. Chen, B. Q. Li, *Fuel*, 2003, **82**, 669–676.
35. P. F. Wang, L. J. Jin, J. H. Liu, S. W. Zhu, H. Q. Hu, *Fuel*, 2013, **104**, 14–21.
36. M. S. Solum, R. J. Pugmire, D. M. Grant, *Energy Fuels*, 1989, **3**, 187-193.
37. P. R. Solomon, M. A. Serio, E. M. Suuberg, *Prog. Energy Combust. Sci.*, 1992, **18**, 133-220.
38. K. Kidena, S. Murata, L. Artok, M. Nomura, *Jpn. Inst. Energy*, 1999, **78**, 869-876.

39. J. L. Figueiredo, M. F. R. Pereira, M. M. A. Freitas, J. J. M. Orfao, *Carbon*, 1999, **37**, 1379–1389.
40. K. Mae, T. Maki, K. Miura, *J. Chem. Eng. Jap.*, 2002, **35**(8), 778-785.
41. P. R. Solomon, M. A. Serio, G. V, *Energy Fuels*, 1990, **4**, 42-54.
42. V. Seebauer, J. Petek, G. Staudinger, *Fuel*, 1997, **76**(13), 1277-1282.
43. L. Giroux, J. P. Charland, J. A. MacPhee, *Energy Fuels*, 2006, **20**, 1988-1996.
44. W. Hodek, J. Kirschstein, K. H. V. Heek, *Fuel*, 1991, **70**, 424-428.
45. Y. Otake, R. G. Jenkins, *Carbon*, 1993, **31**(1), 109-121.
46. Q. L. Zhuang, T. Kyotani, A. Tomita, *Energy Fuels*, 1994, **8**, 714-718.
47. L. H. Zhao, *Master dissertation of Taiyuan University of Technology*, 2007.
48. P. Vinke, M. V. D. Eijk, M. Verbree, A. F. Voskamp, H. V. Bekkum. *Carbon*, 1994, **32**(4), 675-686.
49. U. Zielke, K. J. Huttinger, W. P. Hoffman, *Carbon*, 1996, **34**(8), 983-998.
50. Q. L. Zhuang, T. Kyotani, A. Tomita, *Carbon*, 1994, **32**(3), 539-540.
51. M. Wang, Q. Dong, S. F. Lu, S. S. Tian, G. H. Chen, Y. F. Sun, *J. Chin. Coal Soc*., 2012, **37**(7), 1150-1155.
52. M. F. Li, *Doctoral dissertation of Taiyuan University of Technology*, 2009.
53. S. Porada, *Fuel*, 2004, **83**, 1191–1196.
54. J. X. Liu, X. M. Jiang, J. Shen, H. Zhang, *Energy Convers. Manage.*, 2014, **87**, 1027–1038.
55. E. M. Suuberg, D. Lee, J. W. Larsen, *Fuel*, 1985, **64**, 1668-1671.
56. R. F. Zhao, W. Huang, L. P. Chang, S. Y. Zhu, K. C. Xie, *Coal convers*., 2000, **23**(4), 37-41.
57. T. K. Das, *Fuel*, 2001, **80**, 489–500.
58. V. Strezov, J. A. Lucas, L. Strezov, *J. Anal. Appl. Pyrolysis*, 2004, **71**, 375–392.
59. A. K. Burnham, M. S. Oh, R. W. Crawford, *Energy Fuels*, 1989, **3**, 42-55.
60. L. Qian, S. Z. Sun, D. Wang, H. R. Guo, H. H. Xu, J. Q. Meng, Y. K. Qin, J. Chin. Coal Soc., 2013, **38**(3), 455-460.

Table 3.1. Properties of CC and NCC

Coal	Proximate analysis			Ultimate analysis				
	Moisture wt.%[b]	Ash d-wt.%[c]	Volatile d-wt.%	C d-wt.%	H d-wt.%	N d-wt.%	T-S[a] d-wt.%	Ash-S ash-wt.%
CC	2.2	9.1	23.1	81.2	4.57	1.79	0.51	0.11
NCC	4.9	1.2	48.6	72.8	5.06	0.90	0.13	3.79

[a] T-S, Total sulfur; [b] wt.%, weight percentage; [c] d-, dry coal basis.

Table 3.2. Yields of pyrolysis products of CC and NCC (wt.%[a]).

Coal	Coke	Heavy tar	Light tar	H_2	CH_4	CO	CO_2	H_2O	Balance, %
CC	77.05	6.44	2.19	1.74	3.56	1.80	0.49	4.58	97.86
NCC	52.17	8.94	1.92	1.13	2.29	9.07	7.19	16.89	99.58

[a] wt.%, weight percentage.

Table 3.3. Carbon distribution of NCC, mmol/g-dry coal

Heat treatment temperature, ^{o}C	CH_3	CH_2	Al-O	Bridgehead	Ar-H	Ar-C	Ar-O	COO C=O
Raw	5.1	11.7	2.1	16.0	8.2	6.4	7.0	1.8
400	4.4	7.6	1.6	14.6	8.5	7.0	7.9	1.2
450	3.5	5.2	1.8	13.4	8.4	6.6	6.0	1.0
500	2.3	1.9	0.8	13.0	13.2	6.1	6.5	1.1
600	0.9	1.1	0.5	11.8	17.1	5.6	4.1	1.1
700	0.1	0.1	0.7	8.4	21.8	5.9	2.8	0.6

Table 3.4. Carbon distribution of CC, mmol/g-dry coal

Heat treatment temperature, ^{o}C	CH_3	CH_2	Al-O	Bridgehead	Ar-H	Ar-C	Ar-O	COO C=O
Raw	7.1	7.4	2.2	19.7	17.9	10.1	2.3	0.6
400	6.7	7.5	2.4	20.8	17.4	8.8	1.8	0.5
450	5.1	6.7	2.0	19.5	17.9	9.8	2.8	0.2
500	4.8	3.8	2.1	18.5	26.0	4.4	2.0	0.2
600	1.5	1.4	2.2	16.2	28.2	5.8	1.7	0.4
700	0.6	0.6	0.8	13.5	29.9	8.0	1.6	0.5

Table 3.5. Deconvolution results of NCC and CC

		Assignment	Center Temp., ^{o}C	Gas amount, mmol
a NCC CO	Peak 1	Methoxyl	490	1.63
	Peak 2	Anhydride	592	0.17
	Peak 3	Carbonyl	685	0.15
	Peak 4	Oxygen radical	708	1.46
b CC CO	Peak 1	Methoxyl	494	0.17
	Peak 2	Anhydride	574	0.09
	Peak 3	Carbonyl	725	0.07
	Peak 4	Oxygen radical	731	0.33
c NCC CO_2	Peak 1	Carboxyl	245	0.36
	Peak 2	Ester	407	1.07
	Peak 3	Anhydride	625	0.29
d CC CO_2	Peak 1	Carboxyl	334	0.02
	Peak 2	Ester	489	0.02
	Peak 3	Anhydride	691	0.07
e NCC CH_4	Peak 1	β-methyl	504	1.00
	Peak 2	Aryl methyl	610	0.30
	Peak 3	C_{2+}-hydrocarbon	716	0.20
f CC CH_4	Peak 1	β-methyl	503	0.45
	Peak 2	Aryl methyl	572	1.20
	Peak 3	C_{2+}-hydrocarbon	655	0.63

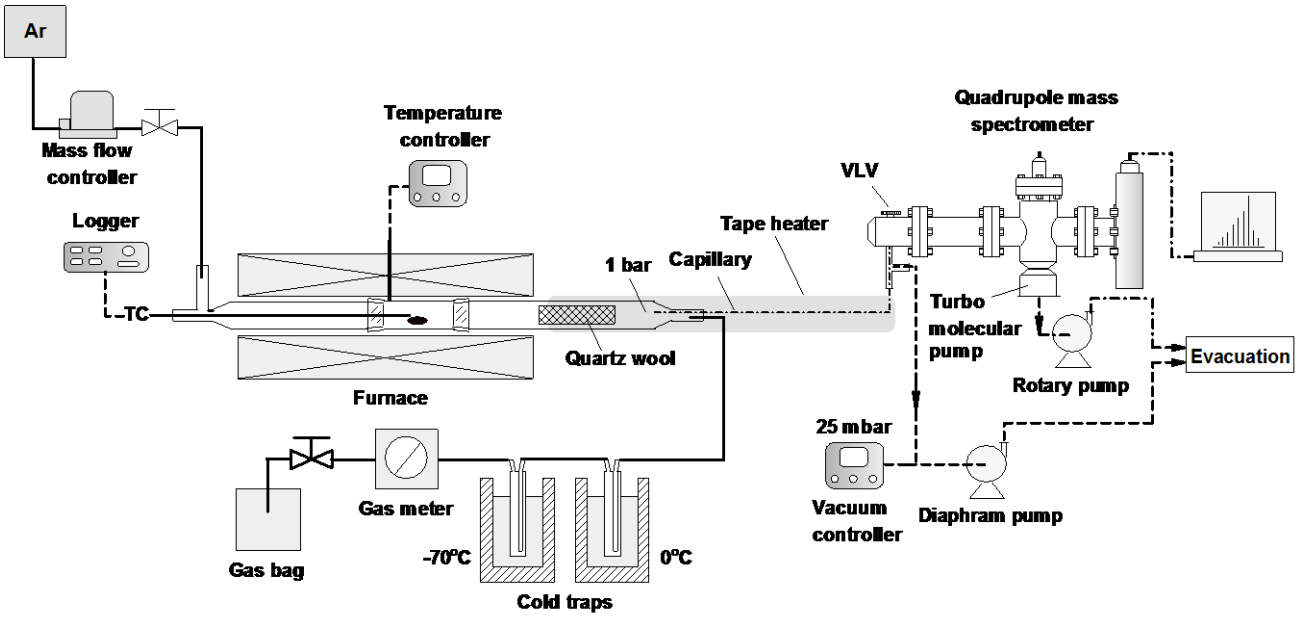

Fig. 3.1. Apparatus of horizontal tube reactor with quadrupole mass spectrometry.

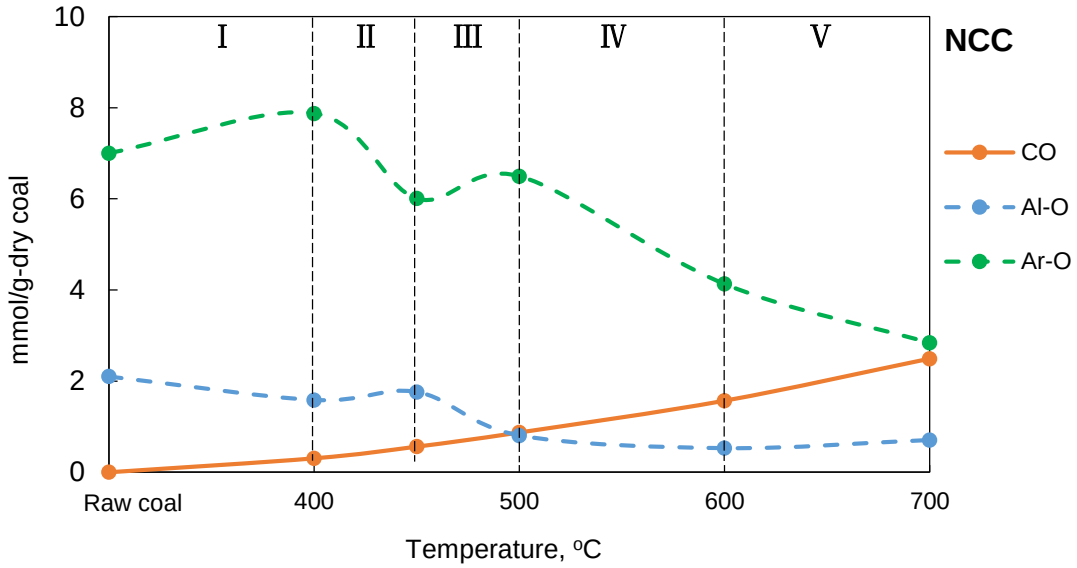

Fig. 3.2. Integrated amount of CO relesed during pyrolysis as a function of temperature and the trends of its relevant functional groups of Al-O and Ar-O of NCC.

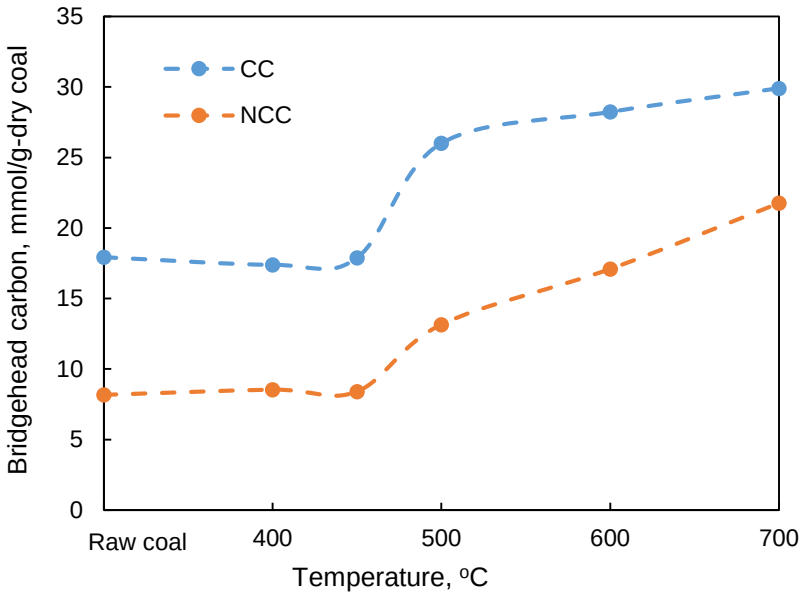

Fig. 3.3. Trends of bridgehead carbons as a function of temperature of CC and NCC.

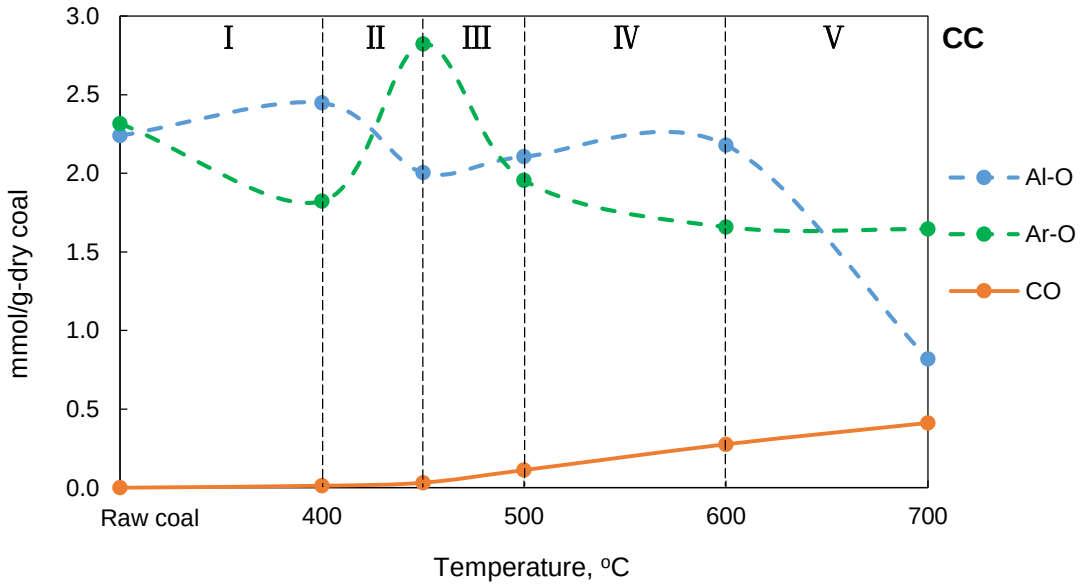

Fig. 3.4. Integrated amount of CO released during pyrolysis as a function of temperature and the trends of its relevant functional groups of Al-O and Ar-O of CC.

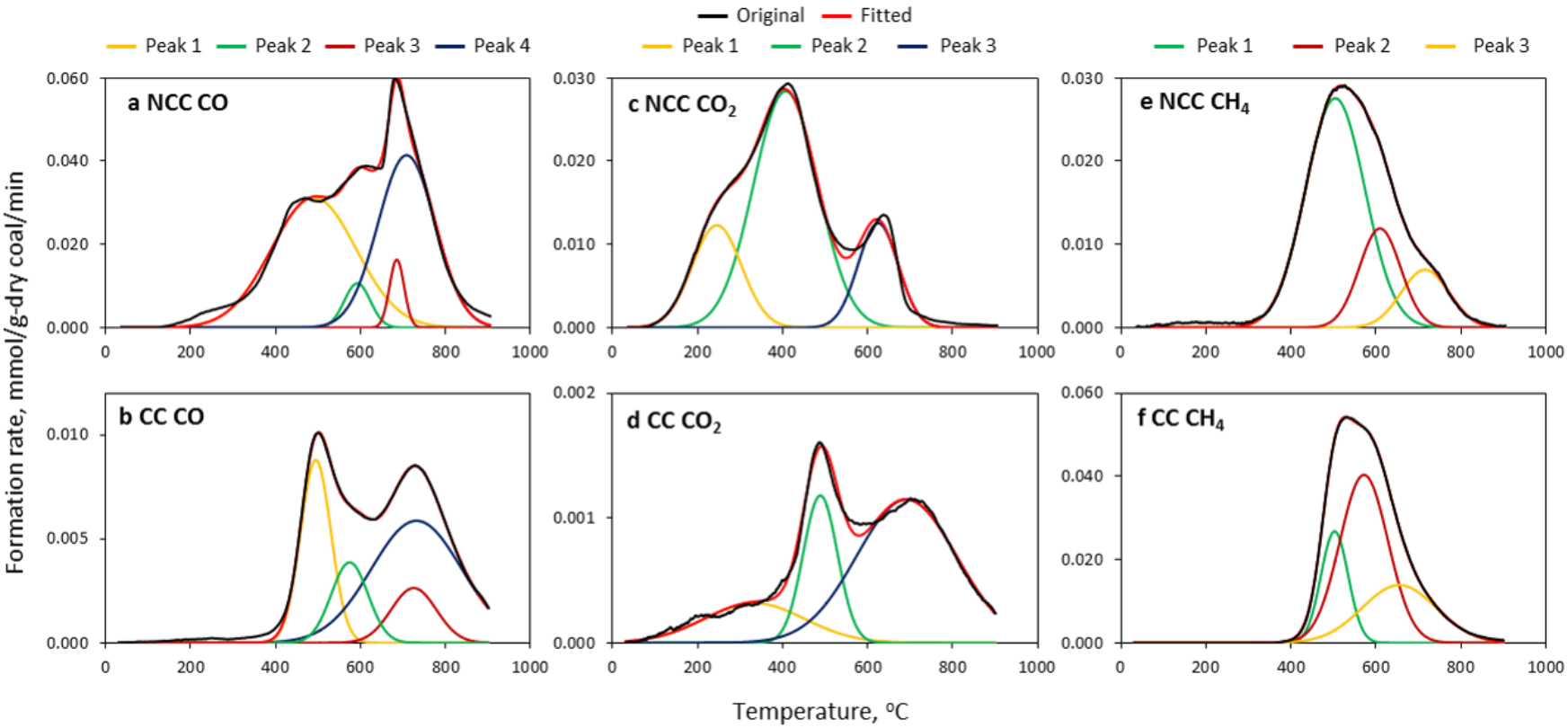

Fig. 3.5. Gas evolutions and deconvolutions as a function of the temperature for NCC and CC.

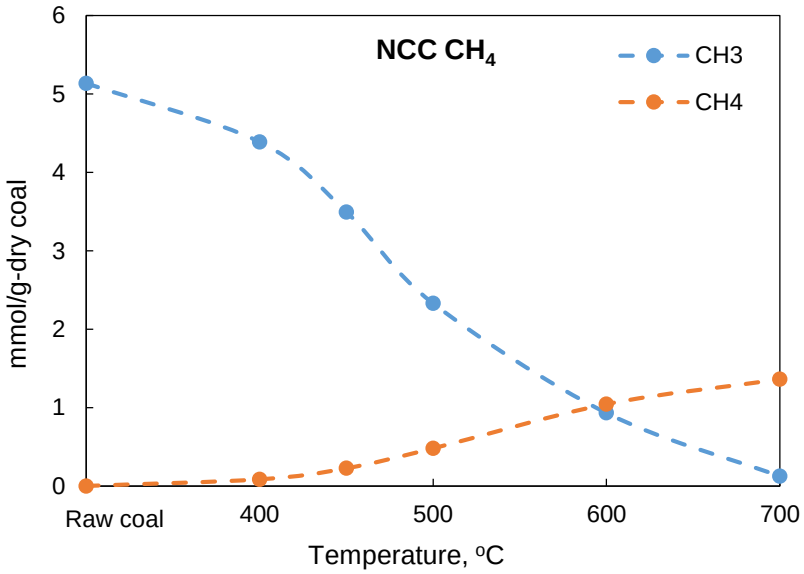

Fig. 3.6. Integrated amount of CH_4 released during pyrolysis as a function of temperature and the trends of its relevant functional groups of -CH_3 of NCC.

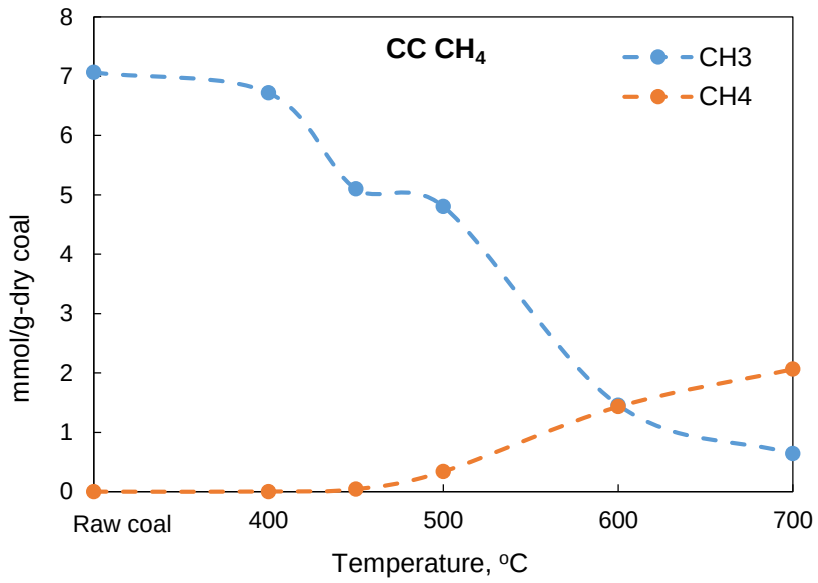

Fig. 3.7. Integrated amount of CH_4 released during pyrolysis as a function of temperature and the trends of its relevant functional groups of -CH_3 of CC.

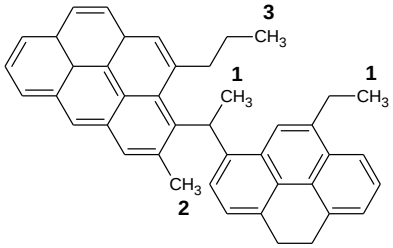

Fig. 3.8. Segmental structure of coal for illustrating different kinds of methyl groups.

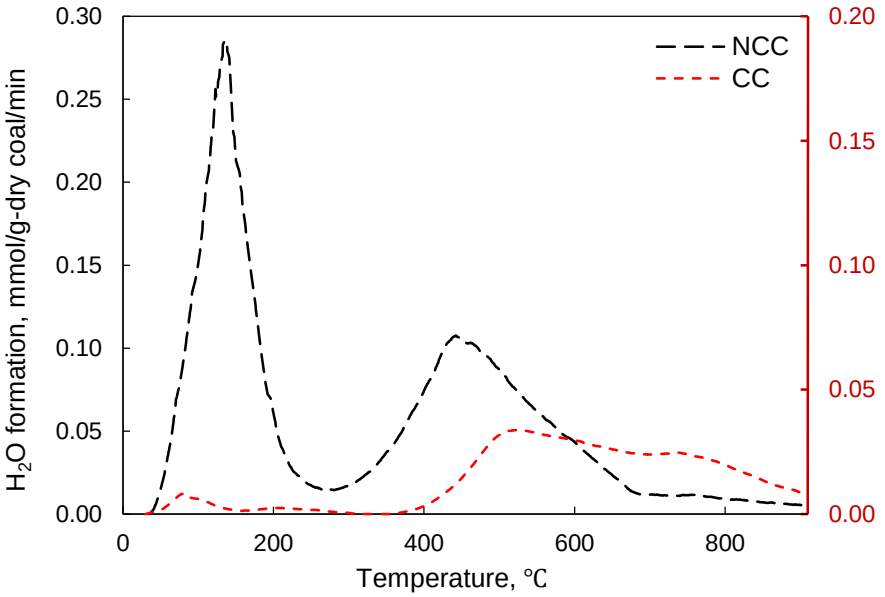

Fig. 3.9. H_2O formation rates as a function of temperature for NCC and CC.

Chapter 4

Real-time analysis of multi-component volatiles from coal pyrolysis with Li^+-attachment ionization mass spectrometry

4.1. Introduction

Gasification is a process that converts solid carbon resources, such as biomass and coal, into fuel gas or syngas. Cold-gas efficiency is one of the most important factors to evaluate the performance of gasification, and therefore, gasification at low temperature has been developed extensively. However, low-temperature gasification often or inevitably allows tar, an undesirable by-product mainly containing the aromatics of macromolecules, to survive through the reactor [1,2].

Tar causes various problems, such as reducing the efficiency of gasification, blocking pipelines, and forming aerosols and soot [3-5]. Such problems make it difficult to perform gasification or downstream processes continuously, safely, and in an eco-friendly manner. Therefore, it is necessary to eliminate tar as much as possible from the reactor and to develop an instrument for its continuous in situ analysis in the product gas.

There are few methods available for the real-time monitoring of the product gas. For example, gas chromatography (GC) method is limited for application to real-time and continuous monitoring because of the duration of time required by per analysis [6]. FT-IR can be used for real-time monitoring, but its sensitivity is too low for some species in tar [7-9]. Compared with other measurement approaches, adopting the mass spectrum (MS) with a quadrupole mass spectrometer is still the best method for accurately monitoring the product gas [10-14]. There are several traditional methods for ionization in the MS, such as electron impact (EI) and chemical ionization (CI). EI is the most conventional ionization method; however, it produces both molecular and fragment ions, making it obviously unsuitable for application to a multi-component system, such as coal/biomass gasification [15]. CI is a lower energy ionization process than EI, producing little or even no fragmentation, but the lack of fragmentation limits the structural information that can be determined about the ionized species [16].

Li^+ ion-attachment mass spectrometry (IAMS) is a soft-ionization method that overcomes the above shortages. IAMS ionization is performed in a non-fragmenting mode by attaching a Li^+ to the monitored molecules. First, a neutral sample molecule becomes an adduct ion by the attachment of a Li^+ with a small amount of energy of less than 2 eV by the Coulomb force. Then, a third-body gas removes any excess energy to stabilize the adducted ion [17]. This technique has the advantage to enable direct determination of unstable, intermediary, and reactive species. In addition, the

sensitivity is high because of ion–molecule reactions [18]. In recent years, IAMS has been studied widely and applied to various research [19-24]. For instance, Li^+ IAMS is used for the continuous measurement of trace amounts of perfluoro compounds and by-products in exhaust gas during semiconductor manufacture [25,26]. It is concluded that Li^+ IAMS exhibiting high sensitivity has the ability to detect 7 ppb c-C_4F_8 molecules in air, as well as to identify compounds by the generation of ions without fragments; this is especially useful for determining molecular weight. In addition, it has been successfully applied to the real-time, continuous measurement of trace organic compounds in air [27], as well as the detection and analysis of free radical species [28-32].

This is the first study that develops a prototype device of Li^+ IAMS for real-time monitoring of aromatics in a simulated tar vapor and real tar vapor from coal pyrolysis. Compared with traditional EI MS, Li^+ IAMS has considerable advantages for monitoring the tar vapor from coal gasification.

4.2. Experimental section

4.2.1. IAMS analysis of simulated tar vapor

IAMS is schematically represented in **Fig. 4.1**. The spectrometer consists of a Li^+-attachment compartment with a Li^+ emitter and an ordinary quadrupole mass spectrometer (L-241G-IA, Canon Anelva Technix Corp.). The Li^+ emitter is prepared with a mixture of Li_2O:Al_2O_3:SiO_2 in a 1:1:1 molar ratio, followed by the calcination at 800-1200 ^oC. The applied voltage to the Li^+ emitter is 10-20 V with an electric current 10^{-7} A. The Li^+ emitting is designed to be localized, such that there will be a region where the kinetic energy of the emitted Li^+ decreases to zero. The amount of sampling gas is adjusted using a variable leak valve (VLV). The sample gas is introduced into the Li^+ ionization chamber and then ionized. Ionized molecules are detected by the quadrupole mass spectrometer with an m/z range of 1-310 amu. The spectrometer is also equipped with an EI emitter, such that ionization can be performed in the EI mode. In this mode, the sample gas is ionized at 70 eV at an emission current of 30 μA. The scan speed is 10 ms/amu for both ion attachment (IA) and EI modes.

This is the first time that IAMS technique is applied to the coal tar monitoring. To make clear the response of the Li^+ IAMS to the coal tar, it is necessary to first monitor a kind of simulated tar which comprises definite organic compounds. Therefore, the simulated tar containing toluene, naphthalene, 2-metylnaphthalene, and 1-naphthol is analyzed in the EI and IA modes. In **Fig. 4.2**, the simulated tar liquid is continuously fed into the vaporizer with a liquid-mass-flow controller at a rate of 0.07 g/min, together with nitrogen as a carrier gas. The liquid is vaporized at 300 ℃ and 300 mbar and introduced into the ionization chamber. The partial pressure of the simulated tar vapor upstream is

varied by controlling the nitrogen-flow rate. The pressure inside the ionization chamber is maintained at 0.5 or 1.0 Pa.

4.2.2. IAMS analysis of real tar vapor produced from coal pyrolysis

A drop-tube reactor (DTR) is heated externally with electric furnaces (**Fig. 4.3**). Dried Loy Yang brown coal with particle sizes ranging from 0.5 to 1.0 mm is used as the coal sample. Particles are continuously fed into the DTR from a screw feeder at a rate of 0.5 or 1.0 g/min, together with a nitrogen flow. The effective gas-residence time in the reactor is about 6 s, and that of the particles is estimated to be 3-4 s at 900 ℃. The products are collected in the train of a char trap with a silica-fiber-made thimble filter, two cold traps, and a gas bag. IAMS is placed between the thimble filter and the first cold trap to introduce a portion of the product gas, such that the introduction of the heaviest portion of tar in the form of aerosol particles can be avoided. The sample gas is introduced into the ionization chamber through a pressure-proof and heat-resistant stainless steel tube (*ca.* 40 cm) with external diameter of 4 mm. Majority of the sample molecules have been pumped out or collected in the gas bag and only very little samples are introduced into the ionization chamber to maintain the vacuum degree. The produced gas is also analyzed in real-time in the IA and EI modes. The pressure of the ionization chamber is fixed at 1.0 Pa. The product collected in the cold traps is analyzed off-line by GC-FID (**Fig. 4.4**). Procedures for the DTR experiments are described elsewhere in detail [33].

4.3. Results and discussion

4.3.1. Simulated tar vapor

A sample containing four types of aromatics (toluene, naphthalene, 2-methylnaphthalene, and 1-naphthol) dissolved in acetone is analyzed as the simulated tar by the EI and IA modes. The operating pressure of the simulated tar vapor is 1.0 Pa. As shown in **Fig. 4.5**, it is difficult to distinguish the molecular ions under the EI mode because all original molecules have been ionized into irregular fragments. For example, it is difficult to confirm the presence of benzene under the interference of toluene, because toluene can be ionized into $^{+}CH_3$ and $^{+}C_6H_5$, which is just one of the ion peaks of benzene. In contrast, Li^{+}-attached molecular ions are formed without fragments and detected exclusively under the IA mode. In addition, the relative intensities of peaks rising from the individual compounds agree well with their relative molar abundances. The molar percentages of these four aromatics are equal to one another in the original sample, and the relative molar ratio of the acetone solvent to any aromatic species is 1.1:1. This indicates the quantitative ionization of these compound molecules by Li^{+} attachment.

Fig. 4.6 exhibits the peak intensities of toluene, naphthalene, 2-methylnaphthalene, and 1-naphthol, with different partial pressures varied by controlling the nitrogen flow in the feed gas. The intensity of each compound increases linearly with its rising partial pressure. The results thus show the validity of IAMS application to real-time and quantitative analysis of tar vapor. In addition, the results in **Fig. 4.6** indicate that the pressure inside the ionization chamber influences the peak intensity, which is simply because the pressure is changed by changing the flow rate of the vapor in the chamber.

4.3.2. Real vapor produced from pyrolysis of coal

Fig. 4.7 shows the result of the IAMS analysis of gas produced by the DTR pyrolysis of coal. Compounds such as benzene, toluene, indene, naphthalene, and methylnaphthalene are detected as Li^+-attached molecular ions; meanwhile, no fragment ions are detected. Molecular ion peaks attached with Li^+ can be easily identified based on the relative molecular mass, which is significantly different from that in the EI mode. Through the comparison between the EI and IA modes in the application of practical pyrolysis, IAMS strongly exhibits qualitative advantages.

To further determine the constituents of tar in the product gas, off-line analysis of GC-FID is performed. As shown in **Fig. 4.8**, compounds containing benzene, toluene, indene, naphthalene, and methylnaphthalene are also detected by GC-FID. The peak areas of GC is proportional to the relative abundances of analyte present in the chromatogram. The relative abundances of these compounds measured by GC-FID are consistent with those measured by IAMS (**Fig. 4.7**). This indicates that IAMS is also viable for quantitative analysis. According to the GC-FID results, some macromolecules with high boiling points are not detected by Li^+ IAMS because of the condensation of tar occurring at the VLV of IAMS; therefore, these large molecules are difficult to be injected into the IAMS equipment.

Fig. 4.9 shows a comparison of the IAMS spectral intensities under different feeding rates of coal. It can be seen that the feeding rate influences the peak intensity. When the feeding rate is changed from 0.5 to 1.0 g/min, the peak intensities are nearly doubled. This result shows the validity of IAMS application to the quantitative analysis of the tar vapor produced from coal pyrolysis.

The prerequisite for using IAMS for quantitative analysis is that the intensity of a molecular ion peak must be independent of the molecular category; in other words, in IAMS, the intensity of the molecular ion peak should not be related to Li^+ affinity. Shiokawa *et al* measured the sensitivities of some species such as CF_4, CHF_3, toluene, chlorobenzene, as functions of Li^+ affinity, where the sensitivity of N_2 is set to 1 [19]. As described in the report, the sensitivites of molecules with low Li^+ affinity (less than 1 eV) increase along with Li^+ affinity. For the molecules with Li^+ affinities above

1 eV, almost all organic compounds have independent sensitivities, except for those with simple molecular structures (such as H_2O and HCHO). It is fortunate that most aromatic molecules in the gas produced by coal prolysis are located in the horizontal zone which means the species have the independent sensitivities. In our study, the sensitivities of some other compounds (naphthalene, 1-naphthol, and 2-methylnaphthalene) to different Li^+ affinities are also measured and found to be equivalent to one another. Li^+ affinities of these three compounds are theoretically calculated by the GAUSSIAN 09 [34] program package at the B3LYP/6-311+G(d,p) level [35,36]. Fully relaxed geometry optimizations and energetic calculations are performed under tight optimization convergence criteria. The vibrational frequencies are calculated at the same basis set levels to identify a local energy minimum (no imaginary frequency). In addition, ultrafine numerical integration grids are used for all calculations. Self-consistent field procedures are performed with tight convergence. The affinity energies are calculated through the following equation:

$$E\ (\text{affinity}) = E\ (\text{molecule}) + E\ (Li^+) - E\ (\text{molecule-}Li^+)$$

Thus, the affinities of Li^+ to naphthalene, 1-naphthol, and 2-methylnaphthalene are 1.78, 1.86, and 1.87 eV, respectively. This calculation level should be sufficient since it has been employed and examined in other studies [31]. The similar IAMS sensitivities of the compounds typically occurring in coal tar can simplify the quantitative analysis of each compound included in multi-component mixtures of tar derived from coal pyrolysis.

4.4. Conclusion

IAMS is applied to real-time monitoring of a simulated tar vapor containing toluene, naphthalene, 2-methylnaphthalene, and 1-naphthol. The results show that the advantages of IAMS (no occurrence of fragmentary ions via the soft attachment of Li^+ ions onto the original aromatic molecules) enables real-time qualitative analysis of the simulated tar vapor. In addition, IAMS performs quantitative analysis of the simulated tar vapor well because of its equivalent sensitivities of the aromatics with Li^+ affinities above 1 eV. Furthermore, the real vapor produced from coal pyrolysis is monitored in real time for the first time by IAMS, and the results coincide very well with those of the simulated tar vapor. This strategy can offer a promising approach in establishing efficient and accurate real-time monitoring of pyrolysis and gasification of carbon resources.

4.5. References

1. T. A. Miline, R. J. Evans, *Technical Report (NERL/TP-570-25357)*, Golden, Colorado, 1998.
2. D. Dayton, *Milestone Completion Report (NERL/TP-510-32815)*, Golden, Colorado, 2002.
3. Y. F. Jia, S. Y. Zhang, Z. H. Cheng, *Coal Conver.*, 2000, **23**, 1-6.

4. J. F. Lu, G. X. Yue, *J. Basic Sci. Eng.*, 1999, **17**, 81-87.
5. B. L. Dou, J. S. Gao, X. Z. Sha, *J. Fuel. Chem. Technol.*, 2000, **28**, 577-579.
6. M. A. Dearth, C. A. Glerczak, W. O. Siegl, *Environ. Sci. Technol.*, 1992, **26**, 1573-1580.
7. M. J. Zhang, B. J. Chen, Z. J. Yu, *Chin. J. Chromatogr.*, 1993, **11**, 1-3.
8. M. J. Zhang, R. S. Tang, S. D. Shen, X. M. He, B. J. Chen, *Chin. J. Chromatogr.*, 1995, **13**, 418-423.
9. M. J. Zhang, S. D. Shen, S. Y. Chen, Y. H. Sun, *Chin. J. Chromatogr.*, 2000, **18**, 241-246.
10. S. D. Richardson, *Chem. Rev.*, 2001, **101**, 211-254.
11. J. Sunner, K. H. Gahm, M. Ikonomou, P. Kebarle, *Combust. Flame*, 1998, **73**, 147-161.
12. R. J. Evans, T. A. Milne, *Energy Fuels*, 1987, **1**, 123-137.
13. R. J. Evans, T. A. Milne, *Energy Fuels*, 1987, **1**, 311-319.
14. P. Hasler, R. Buehler, T. Nussbaumer, *Swiss Federal Office of Energy and Swiss Federal Office for Education and Science*, 1997.
15. M. Y. Dong, Y. H. He, Z. B. Zhu, *J. ECUST*, 2000, **26**, 309-314.
16. A. E. Ashcroft, *RSC*, Cambridge, 1997.
17. H. Okumura, K. Furuya, A. Harata, *J. Phys. D: Appl. Phys.*, 2009, **42**, 065205.
18. T. Fujii, S. Arulmozhiraja, *Int. J. Mass Spectrom.*, 2000, **198**, 15-21.
19. Y. Shiokawa, M. Nakamura, H. Maruyama, Y. Hirano, Y. Taneda, M. Inoue, T. Fujii, *BUNSEKI. KAGAKU*, 2004, **53**, 475-489.
20. S. Takahashi, M. Tsukagoshi, Y. Kitahara, M. Juhasz, T. Fujii, *Rapid Commun. Mass Spectrom*, 2010, **24**, 2625-2630.
21. S. Takahashi, Y. Kitahara, M. Nakamura, Y. Shiokawa, T. Fujii, *Phys. Chem. Chem. Phys.*, 2010, **12**, 3910-3913.
22. M. F. Alif, K. Matsumoto, K. Kitagawa, *Microchem. J.*, 2011, **99**, 394-399.
23. T. Fujii, *J. Therm. Anal. Calorim.*, 2012, **110**, 17-25.
24. M. F. Alif, K. Matsumoto, K. Kitagawa, *Microchem. J.*, 2012, **103**, 179-184.
25. T. Fujii, M. Nakamura, *J. Appl. Phys.*, 2001, **90**, 2180-2184.
26. T. Fujii, S. Arulmozhiraja, *Anal. Chem.*, 2001, **73**, 2937-2940.
27. T. Fujii, P. C. Selvin, M. Sablier, K. Iwase, *Int. J. Mass Spect.*, 2001, **209**, 39- 45.
28. M. Sablier, K. Iwase, G. Sato, T. Fujii, *Chem. Phys. Lett.*, 2005, **409**, 342-348.
29. M. Nakamura, Y. Shiokawa, T. Fujii, M. Takayanagi, M. Nakata, *J. Vac. Sci. Technol. A*., 2004, **22**, 2347-2350.
30. T. Fujii, S. Arulmozhiraja, M. Nakamura, Y. Shiokawa, *J. Appl. Phys.*, 2006, **100**, 084912.
31. T. Fujii, S. Arulmozhiraja, M. Nakamura, Y. Shiokawa, *Chem. Phys. Lett.*, 2006, **425**, 134-137.

32. T. Fujii, *Chem. Phys. Lett.*, 1992, **191**(1, 2) 162-168.

33. L. X. Zhang, T. Matsuhara, S. Kudo, J. I. Hayashi, K. Norinaga, *Fuel*, 2013, **112**, 681-686.

34. M. J. Frisch, G. W. Trucks, H. B. Schlegel, G. E. Scuseria, M. A. Robb, J. R. Cheeseman, G. Scalmani, V. Barone, B. Mennucci, G. A. Petersson, H. Nakatsuji, M. Caricato, X. Li, H. P. Hratchian, A. F. Izmaylov, J. Bloino, G. Zheng, J. L. Sonnenberg, M. Hada, M. Ehara, K. Toyota, R. Fukuda, J. Hasegawa, M. Ishida, T. Nakajima, Y. Honda, O. Kitao, H. Nakai, T. Vreven, J. A. Montgomery, Jr., J. E. Peralta, F. Ogliaro, M. Bearpark, J. J. Heyd, E. Brothers, K. N. Kudin, V. N. Staroverov, T. Keith, R. Kobayashi, J. Normand, K. Raghavachari, A. Rendell, J. C. Burant, S. S. Iyengar, J. Tomasi, M. Cossi, N. Rega, J. M. Millam, M. Klene, J. E. Knox, J. B. Cross, V. Bakken, C. Adamo, J. Jaramillo, R. Gomperts, R. E. Stratmann, O. Yazyev, A. J. Austin, R. Cammi, C. Pomelli, J. W. Ochterski, R. L. Martin, K. Morokuma, V. G. Zakrzewski, G. A. Voth, P. Salvador, J. J. Dannenberg, S. Dapprich, A. D. Daniels, O. Farkas, J. B. Foresman, J. V. Ortiz, J. Cioslowski, and D. J. Fox, *Gaussian, Inc., Wallingford CT*, 2013.

35. A. D. Becke, *J. Chem. Phys.*, 1993, **98**, 5648-5652.

36. R. Ditchfield, W. J. Hehre, J. A. Pople, *J. Chem. Phys.*, 1971, **54**, 724-728.

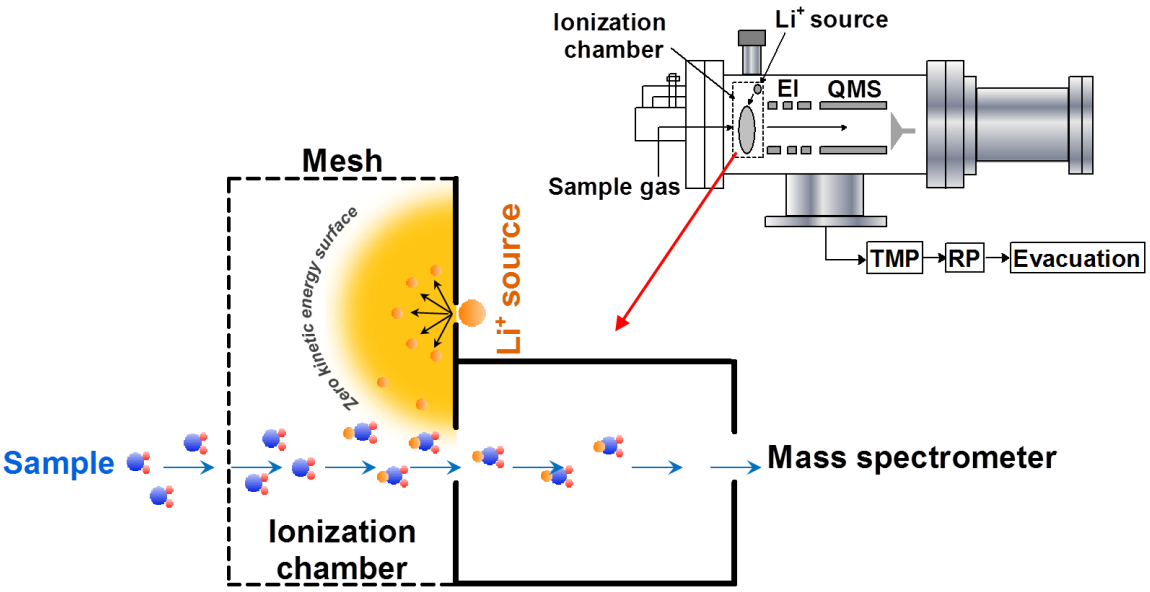

Fig. 4.1. Schematic representation of Li^+-IAMS and the amplified image for the mechanism of Li^+ attachment onto sample molecules at the ionization chamber.

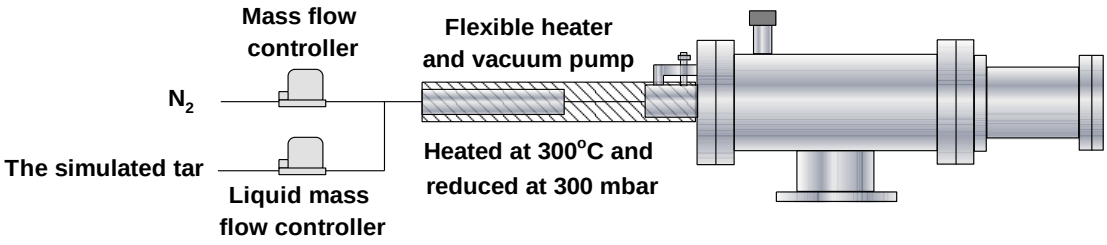

Fig. 4.2. Experimental setup for simulated tar analysis.

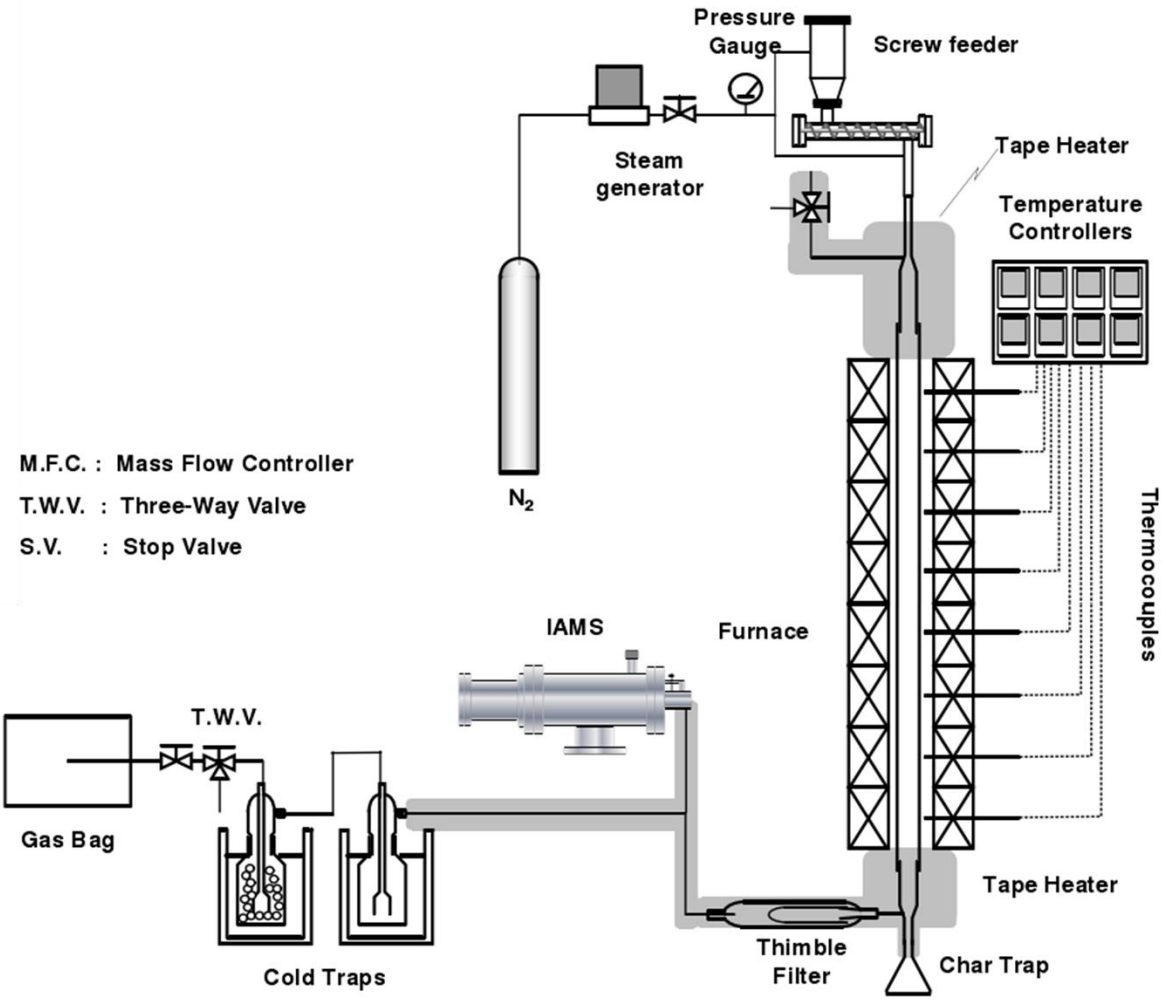

Fig. 4.3. Schematic diagram of the experimental apparatus for in situ tar forming.

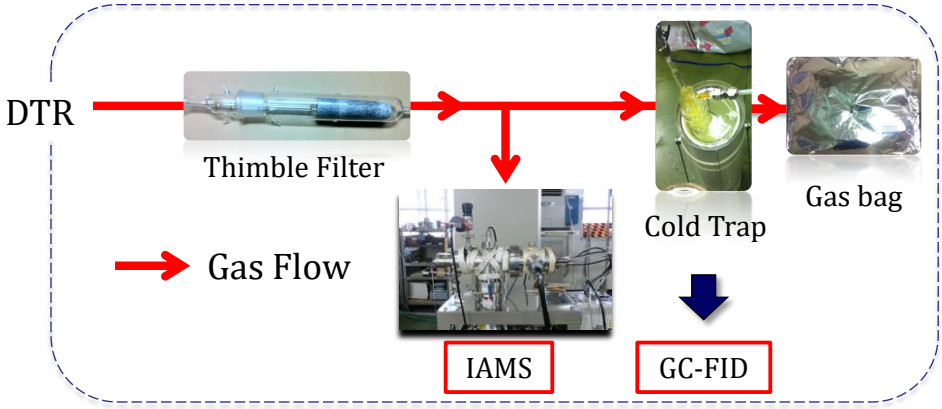

Fig. 4.4. Flow diagram of the experimental apparatus for IAMS analysis and off-line GC-FID analysis.

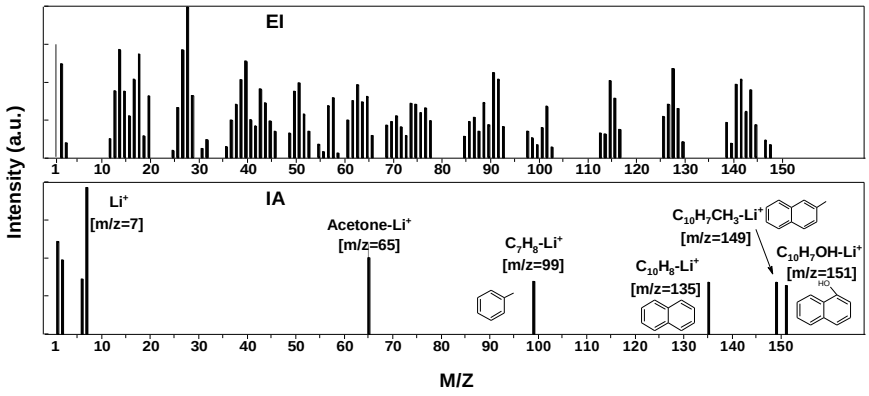

Fig. 4.5. Mass spectra of the simulated tar—toluene, naphthalene, 2-metylnaphthalene, and 1-naphtol—by EI and IA.

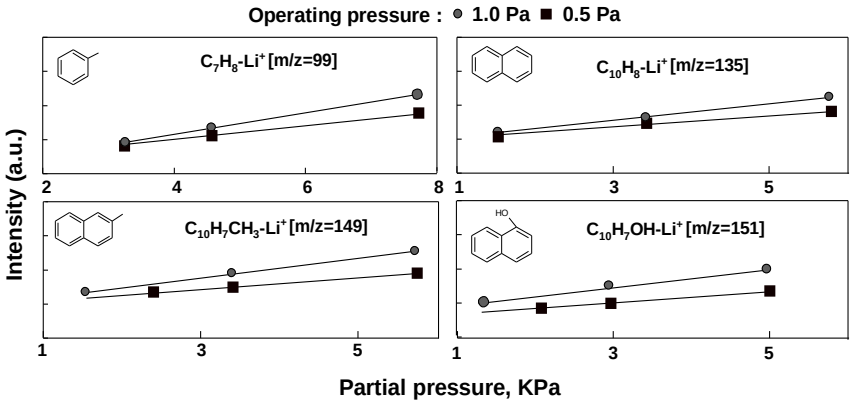

Fig. 4.6. Peak intensity as a function of partial pressure in the feed gas.

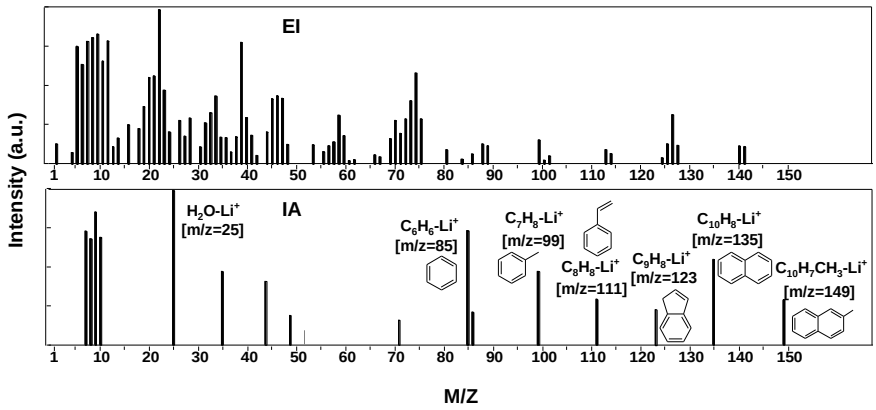

Fig. 4.7. Mass spectra of producer gas from the DTR pyrolysis of coal.

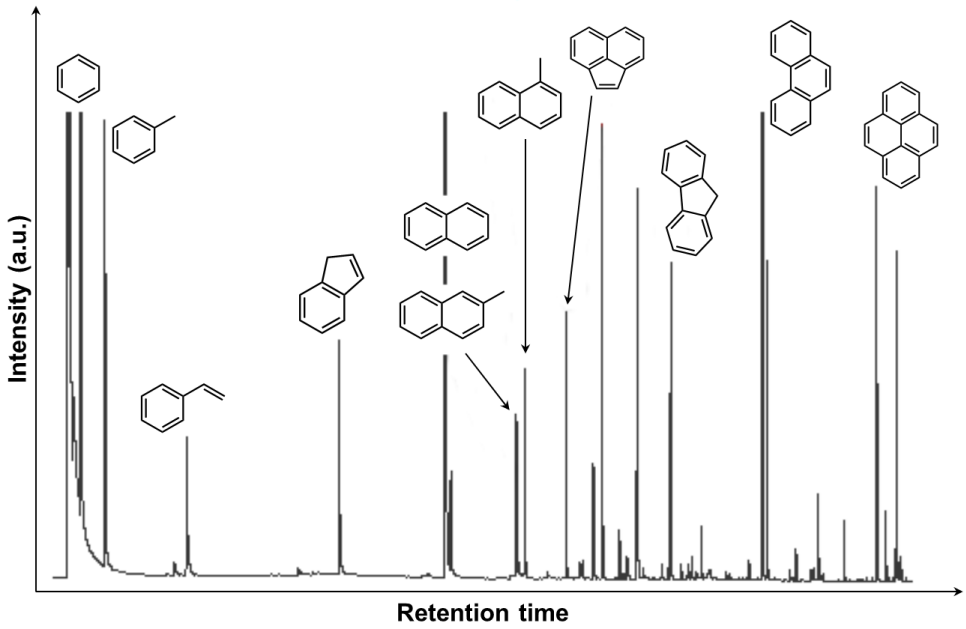

Fig. 4.8. Offline analysis of GC-FID.

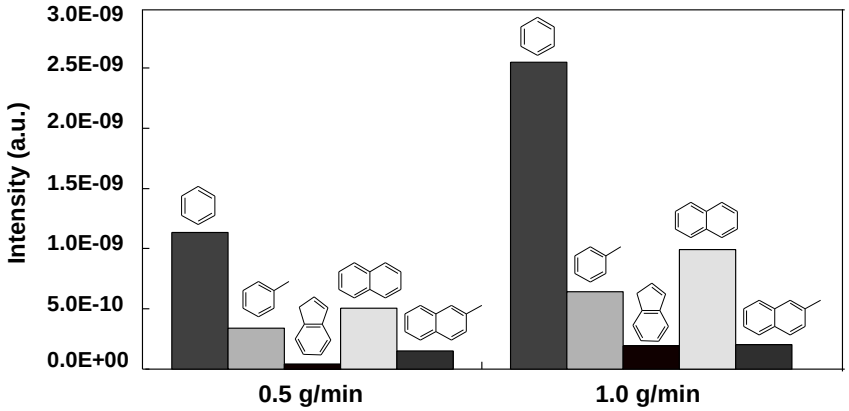

Fig. 4.9. Comparison of IAMS spectra intensities at different feeding rates of coal.

Chapter 5

General Conclusions

The coal pyrolysis process is the initial stage of various thermal transformation processes for coal. The understanding of the coal pyrolysis mechanism will have great guiding significance to the coal conversion process. In the present studies, three main products, i.e., light gases, tar, and char from the coal pyrolysis have been studied for deeper formation mechanism, new monitoring method, and detailed analyzing, respectively. The general conclusion of these works were summarized.

It was found that CC has less substituents, but higher aromaticity and condensation degree than those of NCC based on the solid state ^{13}C-NMR. During pyrolysis, NCC has to be deprived more substituents and produces more gases than CC to evolve an aromatic structure similar to CC. Eventually, it has been impossible to distinguish the coking products of NCC and CC in terms of both aromaticity and condensation degree. Compared with CC, NCC contained more O-containing functional groups, in particular hydroxyl and ester, which were related to the cross-linking reactions during the pyrolysis. It was also found that those reactions related to O-containing groups mainly occur before 500 ℃.

Based on the QMS analysis of the product gases of CC and NCC, and the ^{13}C NMR spectra, the mechanism of coal structure changes at molecular level during pyrolysis were quantitatively revealed that: the CO formation can be mainly attributed to the cleavage of ether group, the removal of anhydrides, oxygen free radicals reaction, and cleavage of carbonyl groups. The removals of carboxyl, ester, and anhydride groups are the main reasons for the CO_2 formation; the quantity of Ar-O during coal pyrolysis will temporarily increase during coal pyrolysis due to the secondary effects of some reactions such as cyclization of side chains containing hydroxyl groups and condensation of O-containing aromatics. The quantity of Al-O increases temporarily as well, because of the migration of O free radicals; the formation of H_2O must be followed by those of CO and CO_2. With the formation of anhydrides, esters, and ethers, the reactions among different carboxyl and hydroxyl groups during coal pyrolysis generate H_2O first, and then their further reactions of removing anhydrides and esters must cause the formations of CO and CO_2; the formation of CH_4 is relatively independent from that of other volatile products. It is generated by the cleavages of β-CH_3, Ar-CH_3, and long chain alkanes attached to the aromatic rings in coal molecules. The dissociation energies of methyls of different locations are greatly different from each other, so the main temperature ranges for CH_4 formation depend largely on the coal ranks. In addition, the different performances of coals with different ranks during pyrolysis are ascribed to their different quantities and distributions of O-containing functional groups, alkyls, and scales of aromatic rings. Representing caking coal, CC has

less substituents, but higher aromaticity and condensation degree than those of NCC representing non-caking coal.

The results of real-time monitoring of a simulated tar vapor measured by IAMS showed that the advantages of IAMS (no occurrence of fragmentary ions via the soft attachment of Li^+ ions onto the original aromatic molecules) enables real-time qualitative analysis of the simulated tar vapor. In addition, IAMS performs quantitative analysis of the simulated tar vapor well because of its equivalent sensitivities of the aromatics with Li^+ affinities above 1 eV. Furthermore, the real vapor produced from coal pyrolysis is monitored in real time for the first time by IAMS, and the results coincide very well with those of the simulated tar vapor. This strategy can offer a promising approach in establishing efficient and accurate real-time monitoring of pyrolysis and gasification of carbon resources.

Acknowledgements

I am especially grateful to my PhD supervisor, Professor Jun-ichiro Hayashi, who did his best to help and encourage me. I would like to thank him for taking over my PhD study in a critical moment. His advice on my research is greatly appreciated. I am very grateful to Professor Koyo Norinaga, who has kindly supported and taught me very much in these years. In addition to Professor Hayashi and Professor Norinaga, Professor Seong-Ho Yoon is much appreciated for serving as my committee members even in the midst of pressing affairs.

I would like to thank Assistant Professor Shinji Kudo for his kindness and great help in the three years. Furthermore, I thank to all laboratory members for their kindness, patience and care, in particular Asuka Mori. We spent a lot of happy time together, and our friendship will be always treasured in the future.

Finally, the financial support of China Scholarship Council (Grant Number 201406420035 and 201406420041) is greatly appreciated.